AGU PUBLICATIONS

JGR

Journal of Geophysical Research: Atmospheres

RESEARCH ARTICLE
10.1002/2014JD021876

Key Points:
- Relation between MJO and different types of SSWs
- Dependence of different SSWs on QBO
- Mechanism how MJO and QBO can influence SSWs

Correspondence to:
C. Liu,
tenkeiliu@gmail.com

Citation:
Liu, C., B. Tian, K.-F. Li, G. L. Manney, N. J. Livesey, Y. L. Yung, and D. E. Waliser (2014), Northern Hemisphere mid-winter vortex-displacement and vortex-split stratospheric sudden warmings: Influence of the Madden-Julian Oscillation and Quasi-Biennial Oscillation, *J. Geophys. Res. Atmos.*, *119*, 12,599–12,620, doi:10.1002/2014JD021876.

Received 6 APR 2014
Accepted 10 OCT 2014
Accepted article online 13 OCT 2014
Published online 28 NOV 2014

Northern Hemisphere mid-winter vortex-displacement and vortex-split stratospheric sudden warmings: Influence of the Madden-Julian Oscillation and Quasi-Biennial Oscillation

Chuanxi Liu[1,2,3], Baijun Tian[1], King-Fai Li[4,5], Gloria L. Manney[6,7], Nathaniel J. Livesey[1], Yuk L. Yung[8], and Duane E. Waliser[1]

[1]Jet Propulsion Laboratory, California Institute of Technology, Pasadena, California, USA, [2]Joint Institute for Regional Earth System Science and Engineering, University of California, Los Angeles, California, USA, [3]Now at Key Laboratory of Middle Atmosphere and Global Environment Observation (LAGEO), Institute of Atmospheric Physics, Chinese Academy of Sciences, Beijing, China, [4]Jack Eddy Fellow, University Corporation for Atmospheric Research, Boulder, Colorado, USA, [5]Department of Applied Mathematics, University of Washington, Seattle, Washington, USA, [6]NorthWest Research Associates, Socorro, New Mexico, USA, [7]New Mexico Institute of Mining and Technology, Socorro, New Mexico, USA, [8]Division of Geological and Planetary Sciences, California Institute of Technology, Pasadena, California, USA

Abstract We investigate the connection between the equatorial Madden-Julian Oscillation (MJO) and different types of the Northern Hemisphere mid-winter major stratospheric sudden warmings (SSWs), i.e., vortex-displacement and vortex-split SSWs. The MJO-SSW relationship for vortex-split SSWs is stronger than that for vortex-displacement SSWs, as a result of the stronger and more coherent eastward propagating MJOs before vortex-split SSWs than those before vortex-displacement SSWs. Composite analysis indicates that both the intensity and propagation features of MJO may influence the MJO-related circulation pattern at high latitudes and the type of SSWs. A pronounced Quasi-Biennial Oscillation (QBO) dependence is found for vortex-displacement and vortex-split SSWs, with vortex-displacement (-split) SSWs occurring preferentially in easterly (westerly) QBO phases. The lagged composites suggest that the MJO-related anomalies in the Arctic are very likely initiated when the MJO-related convection is active over the equatorial Indian Ocean (around the MJO phase 3). Further analysis suggests that the QBO may modulate the MJO-related wave disturbances via its influence on the upper tropospheric subtropical jet. As a result, the MJO-related circulation pattern in the Arctic tends to be wave number-one/wave number-two ~25–30 days following phase 3 (i.e., approximately phases 7–8, when the MJO-related convection is active over the western Pacific) during easterly/westerly QBO phases, which resembles the circulation pattern associated with vortex-displacement/vortex-split SSWs.

1. Introduction

The Northern Hemisphere (NH) stratospheric sudden warming (SSW) strongly disturbs the wintertime extratropical stratosphere [*Andrews et al.,* 1987, and references therein]. When an SSW occurs, the zonal-mean configuration in polar stratosphere is dramatically disrupted, with polar stratospheric temperatures increasing rapidly with time, leading to poleward increase of zonal-mean temperature and, on occasion, a reversal of zonal-mean zonal winds to easterlies. The SSW is defined to be a major warming if the zonal-mean temperature at 10 hPa or below increase poleward from 60°N latitude and the zonal-mean zonal wind reverses [e.g., *Andrews et al.,* 1987]. Observations show that the large stratospheric anomalies associated with mid-winter major SSWs can propagate downward and lead to anomalous weather regimes that may persist as long as two months [e.g., *Baldwin and Dunkerton,* 2001]. *Sigmond et al.* [2013] suggest that accurate modeling of the SSW events can significantly enhance the seasonal forecast skill near the midlatitude surface. In addition, the pronounced variations in the temperature and transport during major SSWs profoundly alter the concentrations and distribution of various trace gases from the upper troposphere through the middle atmosphere [e.g., *Leovy et al.,* 1985; *Manney et al.,* 1994, 2005, 2009; *Liu et al.,* 2009]. Thus, it is important to better understand the dynamics of mid-winter major SSWs and the processes controlling their development and evolution.

During a mid-winter major SSW, the cold stratospheric polar vortex is displaced off the pole and in some cases split. Accordingly, mid-winter major SSWs have been classified into two types: vortex-displacement

(corresponding roughly to those termed "wave number-1") SSWs or vortex-split (typically "wave number-2") SSWs [e.g., *O'Neill*, 2003; *Charlton and Polvani*, 2007 (hereafter CP07)]. Both types of SSWs are associated with an intensified Aleutian High. In addition to the Aleutian High, vortex-split SSWs are usually accompanied by a second anticyclone developing around the Greenwich Meridian at 0°E [e.g., *O'Neill*, 2003]. In addition, these two types of SSWs have different seasonal distributions [e.g., CP07], stratospheric structures [e.g., *Matthewman et al.,* 2009], tropospheric precursors, and surface impacts [e.g., *Mitchell et al.,* 2013]. In terms of precursors, CP07 showed that vortex-displacement (-split) SSWs are predominantly preceded by wave number-1 (-2) upward planetary wave anomalies at 100 hPa. Following the early attempts at connecting the upward planetary wave propagation before SSW events to tropospheric blocking [e.g., *Labitzke*, 1965; *O'Neill and Taylor*, 1979; *Quiroz*, 1986], *Martius et al.* [2009] and *Castanheira and Barriopedro* [2010] investigated tropospheric blocking patterns before different types of SSWs. They showed that vortex-displacement SSWs are nearly always preceded by tropospheric blocking over the Euro-Atlantic sector (wave number-1 pattern), while vortex-split SSWs are typically preceded by tropospheric blocking either over the Pacific sector alone or over both the Euro-Atlantic and Pacific sectors (wave number-2 pattern).

Wintertime planetary wave activity, and thus the occurrence and patterns of SSW events, shows pronounced interannual variability [e.g., *Andrews et al.,* 1987]. Many studies have examined the connections between the SSWs and major modes of climate variability such as El Niño/Southern Oscillation (ENSO), the quasi-biennial oscillation (QBO), and the solar cycle. Early observational studies found a warmer and weaker (cooler and stronger) polar vortex along with an enhanced (weakened) Aleutian high during El Niño (La Niña) [e.g., *van Loon et al.,* 1982; *van Loon and Labitzke*, 1987; *Hamilton*, 1993]. Modeling studies have confirmed the previous results that the El Niño events are associated with enhanced upward propagation of planetary waves from troposphere, and therefore a warmer and weaker stratospheric polar vortex in NH winter [e.g., *Sassi et al.,* 2004; *Manzini et al.,* 2006; *García-Herrera et al.,* 2006; *Bell et al.,* 2009]. In a perpetual January model simulation, *Taguchi and Hartmann* [2006] found enhanced occurrence of SSWs under El Niño conditions over that under La Niña conditions. However, based on reanalysis data, *Butler and Polvani* [2011] found that the SSWs are nearly twice as frequent during ENSO winters as during non-ENSO winters, but with equal probability during El Niño and La Niña winters. *Garfinkel et al.* [2012a] indicated that both ENSO phases are able to disturb the subpolar region of the North Pacific, which is regarded as closely related to SSW precursors. However, they found no preferred ENSO phase for either vortex-displacement or vortex-split SSWs.

The QBO dominates the variability of the equatorial stratosphere (~16–50 km) and is characterized by downward propagation of periodic (~22–34 months) reversals of the zonal mean zonal flow (either easterly or westerly) [e.g., *Baldwin et al.,* 2001]. The QBO can affect the strength of the wintertime stratospheric polar vortex by preventing the equatorward refraction of upward-propagating planetary waves from troposphere in easterly QBO phase and by facilitating the equatorward propagation in the westerly QBO phase. The QBO's modulation of equatorward propagating planetary waves from extratropics is commonly referred to as the "Holton-Tan effect" or "Holton-Tan mechanism" [*Holton and Tan*, 1980, 1982]; recent work has, however, shown this mechanism to be of secondary importance compared to the effect of the mean meridional circulation associated with QBO winds [e.g., *Garfinkel et al.,* 2012c; *Li and Tung*, 2014]. As a result of this QBO modulation, the stratospheric polar vortex is expected to be weaker and warmer in the easterly QBO phase, and stronger and colder in the westerly QBO phase. However, observational results show almost equal frequency of SSWs in each QBO phase [e.g., *Baldwin et al.,* 2001]. Model simulations also indicate that SSWs can occur in either QBO phase as long as the amplitude of upward-propagating waves from the troposphere is large enough [e.g., *Holton and Austin*, 1991]. Moreover, the correlation of SSWs with the QBO also depends on the influence of the 11 year solar cycle. Several studies [e.g., *Labitzke*, 1987; *Labitzke and van Loon*, 1988; *Labitzke et al.,* 2006], recently updated and confirmed by *Labitzke and Kunze* [2009] by examining the last 67 NH mid-winter SSWs, have shown that major mid-winter SSWs preferentially occur during easterly QBO phases and solar minima or during westerly QBO phases and solar maxima. By dividing the observational periods into four groups based on the phases of the solar cycle and QBO, *Camp and Tung* [2007] confirmed that the solar minima and westerly QBO phases are the "least perturbed" state of the winter Arctic stratosphere. However, some outliers do exist (e.g., the 2008–2009 NH winter SSW event occurred during westerly QBO phase and solar minimum). The causes of SSWs are thus still far from understood.

The Madden-Julian Oscillation (MJO) is the dominant form of the intraseasonal variability in the tropical troposphere. It is characterized by slowly (~5 m/s) eastward-propagating, large-scale oscillations in tropical deep convection and in the baroclinic structure of the anomalous wind field [e.g., *Madden and Julian*, 1972;

Table 1. The 3 Month Average (See Text) Standardized Quasi-Biennial Oscillation Index at 50 hPa for the Vortex-Displacement Stratospheric Sudden Warming (SSW) Events

SSW Central Dates	50 hPa
29 Feb 1980	−1.22
04 Dec 1981	−0.26
24 Feb 1984	−0.24
23 Jan 1987	−0.05
15 Dec 1998	−1.01
20 Mar 2000	1.04
16 Dec 2000	−0.14
02 Jan 2002	−0.79
07 Jan 2004	−0.98
21 Jan 2006	−1.75
24 Feb 2007	0.99
22 Feb 2008	−1.77

Zhang, 2005; *Lau and Waliser,* 2012]. The MJO can be predicted with a lead time up to 2–4 weeks and is regarded as an important avenue for bridging the gap between weather forecasting and climate prediction [e.g., *Waliser*, 2012; *Zhang*, 2013]. According to theoretical studies by *Matsuno* [1966] and *Gill* [1980], MJO-related convection can serve as a source for poleward propagating Rossby wave trains in the upper troposphere and lower stratosphere in both hemispheres (i.e., a "Matsuno-Gill" pattern response) [e.g., *Rui and Wang*, 1990; *Hendon and Salby*, 1996; *Kiladis et al.,* 2001]. Further studies have suggested that MJO-related extratropical circulation anomalies can influence extratropical modes such as the Pacific-North-American pattern [e.g., *Simmons et al.,* 1983; *Hsu*, 1996; *Matthews et al.,* 2004; *Mori and Watanabe*, 2008], the North Atlantic Oscillation [e.g., *Cassou*, 2008; *Lin et al.,* 2009], and the Arctic Oscillation [e.g., *Zhou and Miller*, 2005; *L'Heureux and Higgins*, 2008].

Garfinkel et al. [2012b] (hereafter G12) were the first to show a correlation between mid-winter major SSWs and the MJO. They observed that most SSWs tend to follow certain MJO phases (e.g., when the MJO-related convective anomalies are over the equatorial Indian Ocean and/or western Pacific) with certain lag times. They also postulated that the MJO could exert an impact on the stratospheric polar vortex via its influence on the tropospheric North Pacific sector that has previously been shown to be strongly associated with SSWs [e.g., *Nishii et al.,* 2009; *Garfinkel et al.,* 2010, 2012a]. While they did not show evidence of differences in the MJO-SSW relationships between vortex-displacement and vortex-split SSWs, the distinctive characteristics of the two types of SSWs mentioned above make it worthwhile to revisit this issue. In addition, the QBO plays an important role in modulating the upward propagation of planetary waves from the troposphere into and through the stratosphere. Therefore, it is important to examine whether QBO variability can contribute to the two types of SSWs by modulating the MJO-related circulation anomalies.

In this study, we investigate the role of MJO and QBO in modulating the two types of NH mid-winter major SSWs (i.e., vortex-displacement and vortex-split SSWs). In section 2, the data and methods used are described. Section 3.1 shows different MJO-SSW relationships for the two types of SSWs. To understand the different relationships, section 3.2 compares the different features of MJO and the different evolution of OLR anomalies before different types of SSWs. To explore the mechanism by which different characteristics of MJO may contribute to different types of SSWs, section 3.3 compares the circulation pattern related to MJOs with different features (i.e., weak versus strong, incoherent versus coherent eastward propagation) and the differences in the features of MJO before the two types of SSWs. Section 4 examines the dependence of both types of SSWs on the easterly and westerly QBO phases, and the mechanism by which the QBO may influence the two types of SSWs. A summary and discussion are given in section 5.

2. Data and Methods

The central dates of major vortex-displacement and vortex-split SSWs in the past 30 years (1980–2010) are taken from *Cohen and Jones* [2011], based on the National Center for Environmental Prediction-National Center for Atmospheric Research (NCEP-NCAR) reanalysis [*Kalnay et al.,* 1996]. There are 11 vortex-displacement SSWs and 10 vortex-split SSWs, respectively, through 1980–2010 (see their Table 1). According to results of CP07 and *Cohen and Jones* [2011], the identification of SSW types is not sensitive to the reanalysis chosen. However, the vortex-split SSW in February 2001 is not considered in this study because of the uncertainty over its categorization [e.g., CP07; *Cohen and Jones,* 2011]. Following many recent studies [e.g., *Manney et al.,* 2009; *McLandress et al.,* 2013; *Seviour et al.,* 2013], the warming event in January 2006 is regarded as a vortex-displacement SSW in the present study, and not vortex-split as in *Cohen and Jones* [2011].

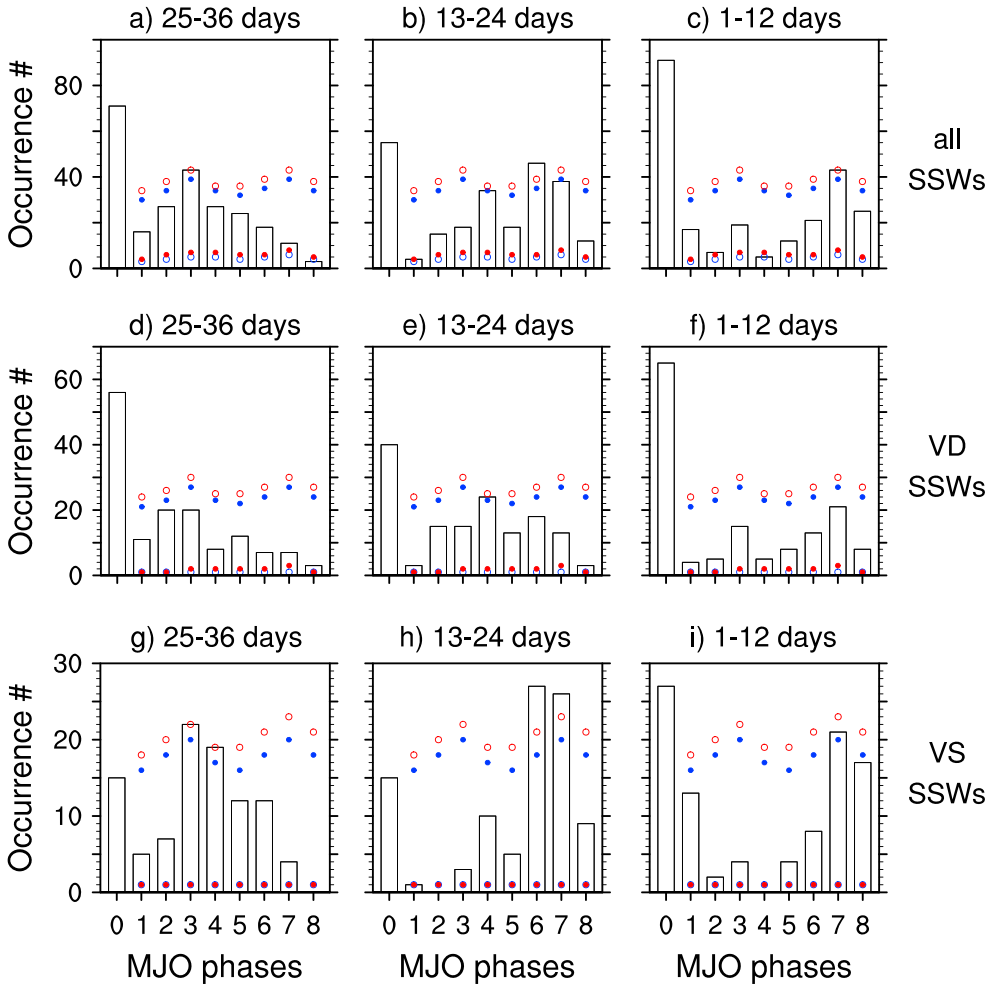

Figure 1. Bars show the number of occurrences of each Madden-Julian Oscillation (MJO) phase during three 12 day periods before all (top), vortex-displacement (center), and vortex-split (bottom) stratospheric sudden warming (SSW) events. Days with the amplitude of Wheeler-Hendon's Real-time Multivariate MJO (RMM) index [*Wheeler and Hendon*, 2004] below 1.0 are marked as the MJO phase 0. Based on a two-tailed Monte Carlo test (see text), the blue and red circles mark the 2.5% and 97.5% percentiles, while the red and blue dots mark the 5% and 95% percentiles.

The MJO events and phases are determined by the real-time multivariate MJO (RMM) index [*Wheeler and Hendon*, 2004]. The daily values of RMM1 and RMM2 are obtained from the Australian Bureau of Meteorology website (http://cawcr.gov.au/staff/mwheeler/maproom/RMM/). RMM1 and RMM2 were calculated by projecting the combined fields of 15°S–15°N meridionally averaged satellite-observed outgoing longwave radiation (OLR) and zonal winds at 850 and 200 hPa onto the two leading empirical orthogonal function structures derived using the same meridionally averaged variables. The time series of RMM1 and RMM2 vary mostly on intraseasonal timescales, and the associated three-dimensional flow structure captures the MJO variability. Based on the RMM index, lifecycles of the MJO can be divided into eight phases indicating the geographic location of the MJO-related convective anomalies from tropical Indian Ocean toward equatorial western Pacific. In phases 8 and 1, convection of a decaying MJO event is present in the central Pacific, while enhanced convection of a growing event is evident over Africa and the equatorial western Indian Ocean. Over the subsequent phases, convection builds in the Indian Ocean (phases 2–3) and propagates eastward toward the Maritime Continent (phases 4–5) and then equatorial western Pacific (phases 6–7). The MJO is regarded to be active if its amplitude $[(RMM1^2+RMM2^2)^{1/2}]$ is greater than 1.0. Otherwise, it is marked as phase 0 (see Figures 1 and 2). Sensitivity analysis suggests that our results are not qualitatively dependent on this threshold. Any period (either with 6 day or 12 day interval) shown in Figures 1 and 2 is regarded as a MJO active period if there is at least one MJO phase whose number of days is larger than or comparable to that of

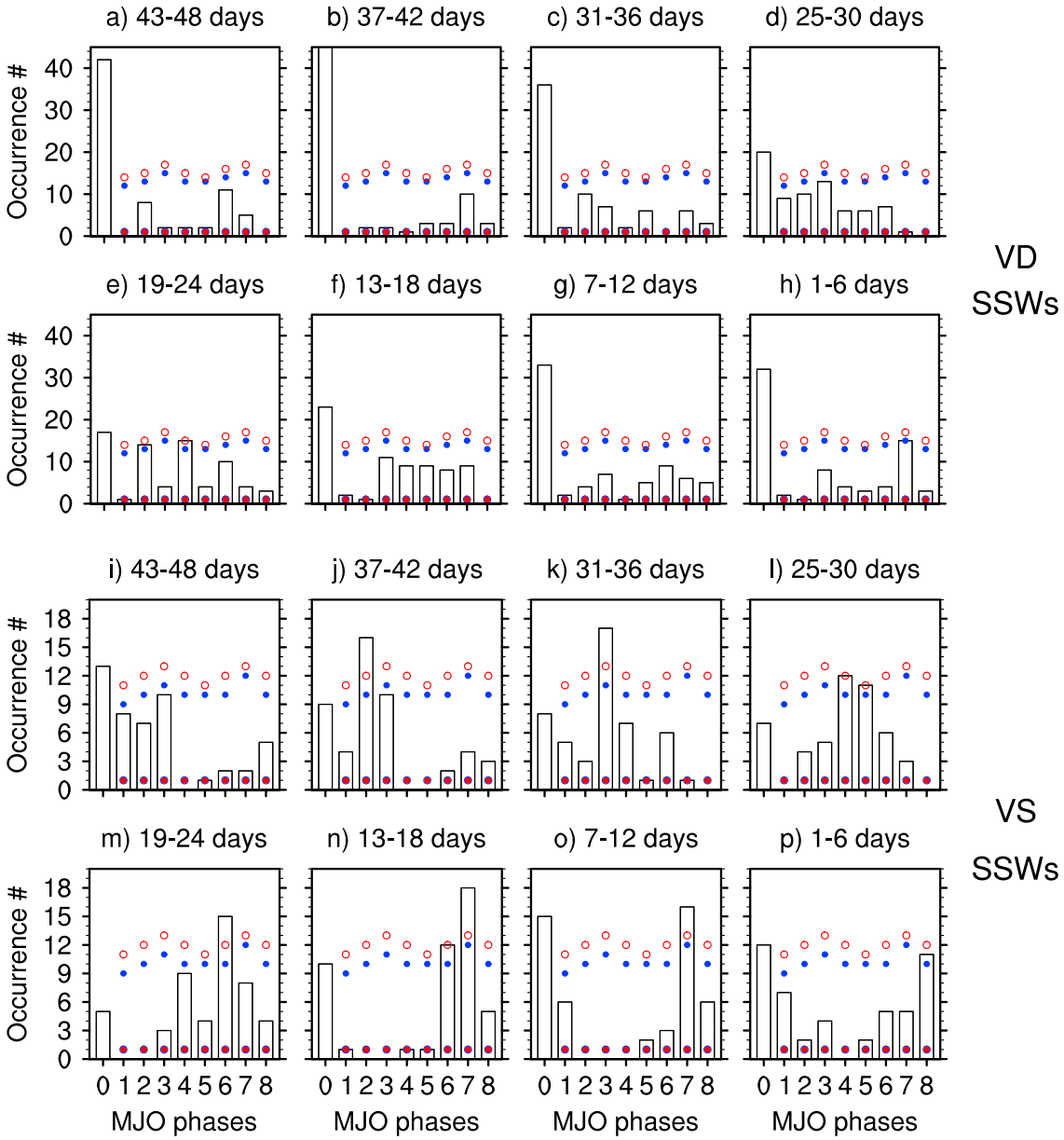

Figure 2. Same as Figure 1, but for eight 6 day intervals before vortex-displacement (top) and vortex-split (bottom) SSWs.

phase 0. Recent studies [e.g., *Straub*, 2013; *Kiladis et al.*, 2014] have suggested that RMM index is heavily circulation based. Therefore, we have repeated our analysis using the more convection-based MJO index (e.g., OLR-based MJO index (OMI) described by *Kiladis et al.* [2014]). The results based on OMI (not shown) and RMM indices are generally similar, with a slight phase difference.

The daily mean OLR observed by the Advanced Very High Resolution Radiometer instrument aboard the NOAA's polar orbiting spacecraft [e.g., *Gruber and Krueger*, 1984; *Liebmann and Smith*, 1996] and geopotential height from the NCEP-NCAR reanalysis at a horizontal resolution of 2.5° × 2.5° are also used. To derive the daily anomalies, the long-term daily climatology is removed from the daily means. A 20–100 day band-pass filter is further applied to derive the MJO-related daily anomalies.

The monthly standardized 50 hPa QBO index (1979–2010) obtained from NOAA's Climate Prediction Center (at http://www.cpc.ncep.noaa.gov/data/indices/) is used to determine the equatorial QBO phases for each SSW event. In the present study, the easterly (westerly) QBO phase is defined when the 50 hPa QBO index is less (greater) than 0 m/s. Results based on the 30 hPa QBO index are qualitatively the same, and thus are not shown.

The horizontal components of the wave-activity flux vector [*Takaya and Nakamura*, 2001] have been used to illustrate the wave activity at 100 hPa after certain MJO phases [e.g., *Lin et al.,* 2009]. The wave-activity flux (W) is defined as:

$$W = \frac{p\cos\phi}{2|U|}\begin{pmatrix} \frac{U}{a^2\cos^2\phi}\left[\left(\frac{\partial\psi'}{\partial\lambda}\right)^2 - \psi'\frac{\partial^2\psi'}{\partial\lambda^2}\right] + \frac{V}{a^2\cos\phi}\left[\frac{\partial\psi'\partial\psi'}{\partial\lambda\,\partial\phi} - \psi'\frac{\partial^2\psi'}{\partial\lambda\partial\phi}\right] \\ \frac{U}{a^2\cos^2\phi}\left[\frac{\partial\psi'\partial\psi'}{\partial\lambda\,\partial\phi} - \psi'\frac{\partial^2\psi'}{\partial\lambda\partial\phi}\right] + \frac{V}{a^2}\left[\left(\frac{\partial\psi'}{\partial\phi}\right)^2 - \psi'\frac{\partial^2\psi'}{\partial\phi^2}\right] \\ \frac{f^2}{N^2}\left\{\frac{U}{a\cos\phi}\left[\frac{\partial\psi'\partial\psi'}{\partial\lambda\,\partial z} - \psi'\frac{\partial^2\psi'}{\partial\lambda\partial z}\right] + \frac{V}{a}\left[\frac{\partial\psi'\partial\psi'}{\partial\phi\,\partial z} - \psi'\frac{\partial^2\psi'}{\partial\phi\partial z}\right]\right\} \end{pmatrix}, \quad (1)$$

where a is the earth's radius, $z = -H\,lnp$, where p = (pressure/1000 hPa) and H is a constant scale height, and $N^2 = (R_a p^{\kappa}/H)(\partial\theta/\partial z)$ is the buoyancy frequency squared where θ denotes potential temperature, R_a is the gas constant of dry air, and κ is defined as R_a normalized by the specific heat of air for constant pressure. (ϕ, λ) are latitude and longitude, respectively. The geostrophic streamfunction is defined as $\psi = \Phi/f$, where Φ is geopotential and $f(=2\Omega\sin\phi)$ is the Coriolis parameter with the earth's rotation rate Ω. The quantities with primes indicate the deviations from the monthly climatology. $U = (U, V, 0)^T$ denotes the steady zonally inhomogeneous basic flow. In the present study, the same diagnostic is applied to characterize the wave activity associated with different types of SSWs and those associated with certain MJO phases (phases 7–8) in both easterly and westerly QBO phases.

To determine the significance of the relationship between MJO phases and SSWs (as shown in Figures 1 and 2), a two-tailed Monte Carlo test is performed by first dividing all of the extended NH winters (November–April, 1980–2010) into 12 day and 6 day intervals (corresponding to the 12 day and 6 day intervals used in the MJO analysis described above). Sets containing representative numbers (12, 8, and 20) of these short periods are randomly selected (corresponding to the 12 vortex-displacement SSWs, 8 vortex-split SSWs, and 20 SSWs totally) in which to calculate the number of occurrences of each MJO phase. Five thousand similar sets are generated in a Monte Carlo procedure to derive the eight "climatological" distributions of each MJO phase. Finally, the "climatological" distributions of the MJO phases are used to determine the 90% and 95% significance levels of the results shown in Figures 1 and 2 based on the percentile (e.g., 2.5%, 5%, 95%, and 97.5%) of each MJO phase. The MJO-related composites are calculated from data that are highly filtered and thus have substantial autocorrelations, making the effective sample size smaller than the actual number of samples. Therefore, as in previous studies [e.g., *Weare*, 2010; *Lin et al.,* 2009; *Tian et al.,* 2011], a two-tailed Student's t test with reduced degrees of freedom is performed to determine the significance of the composite OLR anomalies associated with each MJO phase. Similar to *Lin et al.* [2009], the effective sample size of the MJO-related anomalies is estimated as follows:

$$N' = N\left(\frac{1 - r_1 r_2}{1 + r_1 r_2}\right), \quad (2)$$

where N' is the effective sample size, N is the original sample size, and r_1 and r_2 are the autocorrelation of RMM1 and RMM2 with 2 day lag. Since the autocorrelation coefficients of RMM1 and RMM2 with 2 day lag are both around 0.91, $N' = 0.089 \times N$. This value is equivalent to 1/11.4, which has been used in previous studies [e.g., *Tian et al.,* 2011]. Since the autocorrelation coefficient of the 50 hPa monthly QBO index with 2 month lag is around 0.82, we have $N' = 0.19 \times N$ assuming that $r_1 = r_2$.

To explore the mechanisms by which MJOs with different features may contribute to each type of the SSW, we have examined the circulation pattern related to weak and strong MJOs and that related to MJOs with incoherent and coherent eastward propagation. Weak MJOs are defined as those with RMM index greater than 1.0, but smaller than 1.5. Strong MJOs are defined as those with RMM index greater than 1.5. The results are not qualitatively dependent on the threshold we selected. Considering the high day-to-day variability in the propagation and intensity of the MJO, the daily mean RMM indices are averaged for five consecutive days to construct a 5 day mean RMM index [e.g., *Lin et al.,* 2009] in order to define the incoherence or coherence of eastward propagating MJOs. MJOs with incoherent eastward propagation are defined as those with persistent eastward propagation (without change of direction) for less than 30 days or for less than or equal to four phases within 30 days. Conversely, MJOs with coherent propagation are defined as those with

persistent eastward propagation (without change of direction) for more than 30 days and for more than four phases. For MJOs with incoherent and coherent propagation, the amplitude of the RMM index must remain larger than 1.0. As a result, we obtain 42 incoherent eastward propagating MJO events and 20 coherent eastward propagating MJO events in total during the boreal winters (December–February) between 1980 and 2010. Sampling of the incoherent MJO events is by definition independent of that of the coherent events. The comparison between incoherent and coherent MJO events suggests that the incoherent MJOs are usually weaker than coherent events (not shown).

3. Different MJO-SSW Relationships for Different Types of SSWs

3.1. Different MJO-SSW Relationships

To illustrate the relationship between MJO and SSWs, G12 examined the MJO phases for three different periods preceding the central dates of the SSWs with a 12 day interval (25–36, 13–24, and 1–12 days prior to the SSWs) (see their Figure 1). We first perform a similar analysis (top panels in Figure 1) and then extend it to look at the different types of SSWs separately (center and bottom panels in Figure 1). To make the result more straightforward, we do not normalize the values in Figure 1 by a climatology as done by G12. As shown in Figures 1a–1c, the dominant MJO phase shifts from phase 3 (Figure 1a) to phase 6 (Figure 1b), and finally to phase 7 (Figure 1c) throughout the three 12 day periods before the SSW central dates. Based on the two-tailed Monte Carlo test, all three peaks are significant at the 95% confidence level, which is generally consistent with Figure 1 of G12. It suggests that there is pronounced MJO activity (that is, with large intensity and coherent eastward propagation) throughout the 36 days prior to the SSWs. However, when a similar analysis is applied to the two different SSW categories separately, the resulting MJO-SSW relationships are distinct (compare Figures 1d–1f with 1g–1i). First, the distribution of the dominant MJO phases prior to vortex-split SSWs is highly similar to that for all SSWs shown in the top panels in Figure 1, but this is not the case for vortex-displacement SSWs (compare center and top panels in Figure 1). Despite the small sample of vortex-split SSWs, almost all the MJO phase peaks shown in Figures 1g–1i are significant at the 95% confidence level, except for the MJO phase 7 in Figure 1i, which is significant at the 90% confidence level. In contrast, for vortex-displacement SSWs, the only MJO phase peak that is significant is phase 4 13–24 days before the events (Figure 1e). The number of occurrences of different MJO phases also varies much more strongly for vortex-split SSWs than for vortex-displacement SSWs. Additionally, the number of occurrences of peak MJO phases before SSWs is larger than or comparable to that of the MJO inactive phase (phase 0) for vortex-split SSWs but much smaller than that of the MJO inactive phase for vortex-displacement SSWs (compare center and bottom panels in Figure 1). This indicates that MJOs before vortex-split SSWs are much more active (with larger intensity and more coherent eastward propagation) than those before vortex-displacement events. Figure 1 demonstrates that the MJO-SSW relationship obtained by G12 arises primarily from vortex-split SSWs.

Given that the typical transition time between each of the numbered MJO phases is about 6 days [*Wheeler and Hendon*, 2004], we perform an analysis similar to that in Figure 1, but with a time interval of 6, instead of 12, days, as shown in Figure 2. Before vortex-displacement SSWs, the MJO phase 0 is mostly dominant throughout the eight periods with most of the remaining MJO phases below the 90% confidence level, indicating the MJO activity is overall weak (see Figures 2a–2h). We note that some peaks of the MJO phases (e.g., phases 2, 4, and 7) are above the 90% but still below the 95% significance level during some periods, suggesting that the MJO becomes relatively active in certain phases/regions (see Figures 2e and 2h). In contrast, before vortex-split SSWs, there are seven MJO active periods during which peak MJO phases are significant at the 95% and/or 90% confidence levels with a much larger number of occurrences than the MJO phase 0 (Figures 2j–2p), indicating much more active MJO during those periods. In contrast to the case before vortex-displacement SSWs, the distribution of peak MJO phases shows the same tendency to move from early phases (e.g., phases 2–5 in Figures 2j–2l) toward late phases (e.g., phases 6–8 in Figures 2m–2p) that was seen in Figures 1a–1c and 1g–1i. This confirms the results from Figure 1 that the MJO-SSW relationship obtained by G12 arises primarily from vortex-split SSWs. Our results in this section indicate that the MJO may have a much stronger impact on vortex-split SSWs than on vortex-displacement SSWs.

3.2. Understanding the Different MJO-SSW Relationships

To understand the different MJO-SSW relationships shown in Figures 1 and 2, the features of the MJO-related anomalies are compared for different types of SSWs. Figure 3 shows the composite of band-pass-filtered

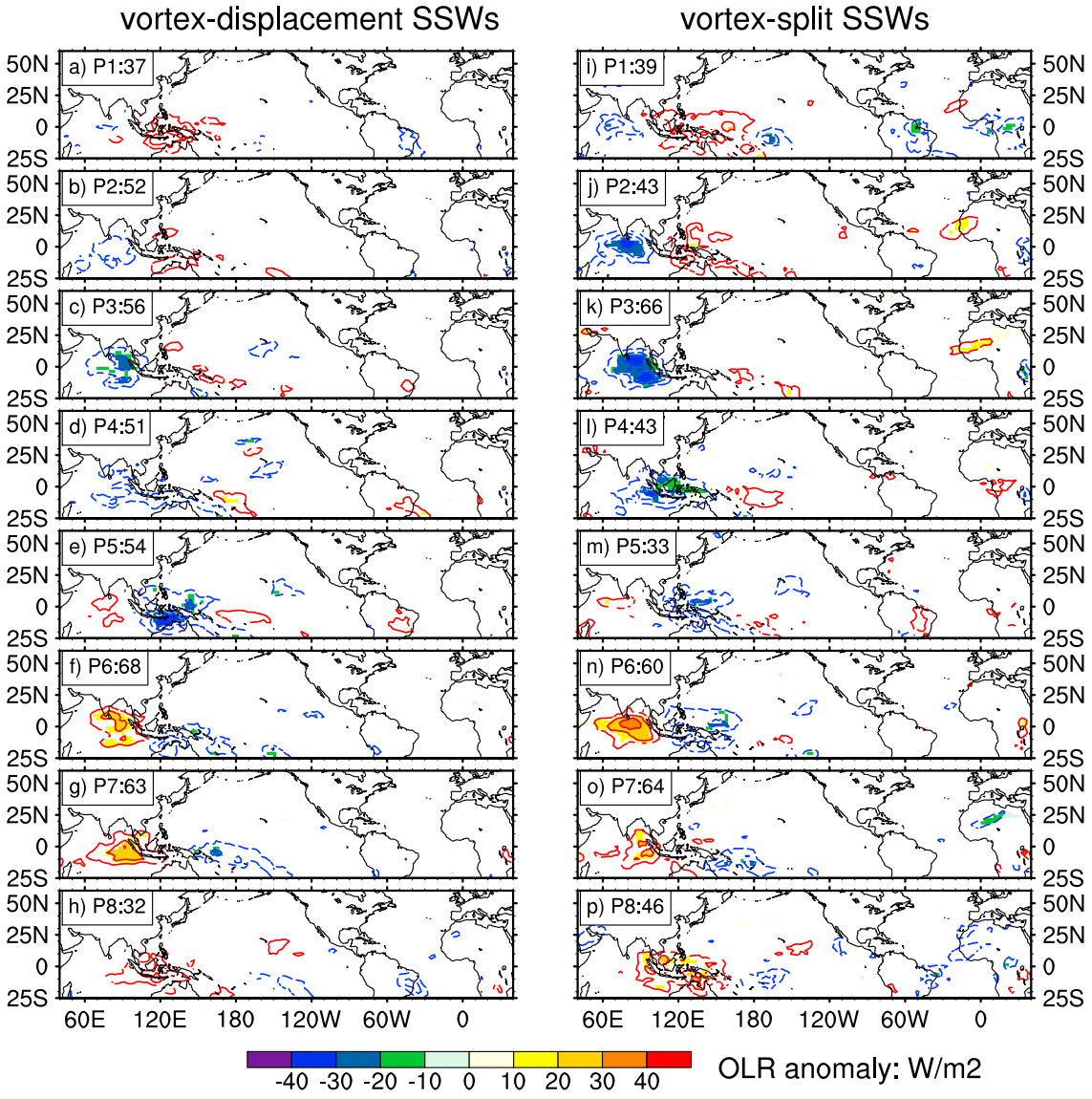

Figure 3. Composite of band-pass-filtered (20–100 days) outgoing longwave radiation (OLR) anomaly (unit: W/m^2) related to each MJO phase between 50 days before and 10 days after the central dates of vortex-displacement (left) and vortex-split (right) SSWs. Only days with RMM amplitude greater than 1.0 are included. The number shown in each panel represents number of days used to construct each composite. Positive and negative anomalies that are statistically significant at the 90% confidence level based on a regular Student's *t* test are indicated by red solid and blue dashed contours. The contour interval is 10 W/m^2. The shaded areas are statistically significant at the 90% confidence level based on a two-tailed Student's *t* test with reduced degrees-of-freedom (see text).

(20–100 days) OLR anomalies associated with each MJO phase between 50 days before and 10 days after the SSW central dates. In the composite, only the MJOs whose amplitude is greater than 1.0 are considered. Because a two-tailed Student's *t* test with reduced degrees-of-freedom was applied, only a small portion of the MJO-related anomalies are shown. Compared to the anomalies during vortex-displacement SSWs, the MJO-related OLR anomalies during vortex-split SSWs are stronger over the equatorial Indian Ocean and Maritime Continent (compare Figures 3j–3l, 3n, and 3p to Figures 3b–3d, 3f, and 3h). It is also noted that there are similar differences in the OLR anomalies over equatorial Atlantic and North Africa (compare Figures 3j–3k and 3o–3p to Figures 3b–3c and 3g–3h). Daily evolution of the RMM indices for each SSW event (not shown) supports the information given by our composites, indicating that the MJOs are weaker with more incoherent eastward propagation before vortex-displacement SSWs, but stronger with more coherent eastward propagation before vortex-split SSWs.

Figure 4 compares the evolution of 6 day mean daily OLR anomalies (i.e., with the daily climatology removed from the daily mean) up to 48 days prior to the central dates of both types of SSWs. For vortex-split SSWs, there

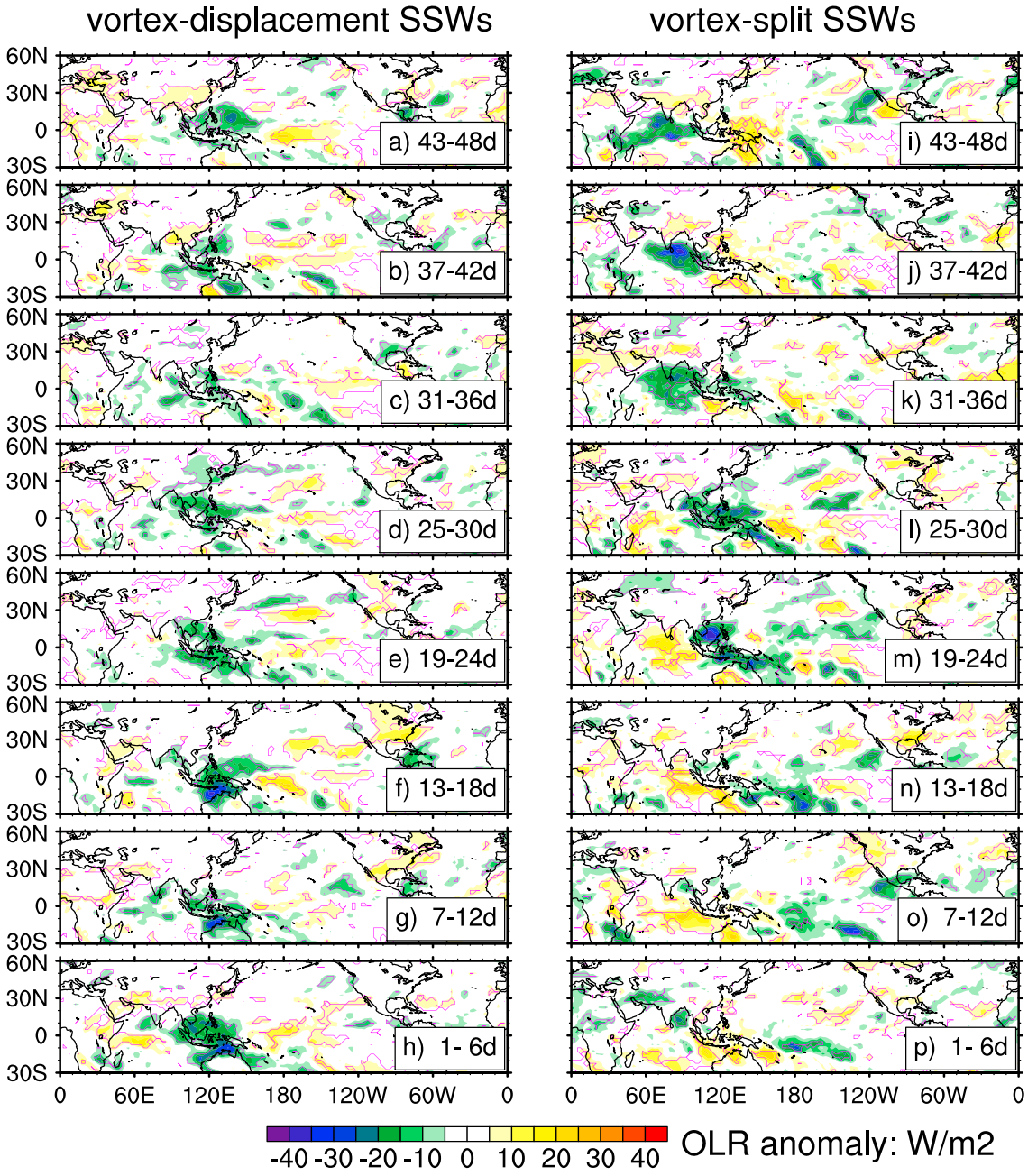

Figure 4. Composite of OLR anomalies (i.e., with the daily climatology removed from the daily mean) up to 48 days prior to the central dates of vortex-displacement (left) and vortex-split (right) SSWs with 6 day interval. The magenta solid lines mark the areas that are statistically significant at the 95% confidence level based on a two-tailed Student's *t* test.

are pronounced MJO-like eastward propagating OLR anomalies moving from the equatorial Indian Ocean toward the equatorial western and central Pacific (right panels in Figure 4). Despite the fact that no band-pass filter has been applied, strong MJO-like OLR anomalies are seen along the Equator (see Figures 4i–4p, similar to MJO phases 2–8 as indicated in Figure 2). In contrast, for vortex-displacement SSWs, the negative OLR anomalies over the Maritime Continent and the equatorial western Pacific are weak prior to 30 days before the SSW central dates (see Figures 4a–4c). Closer to the SSW central dates, the relatively stationary negative OLR anomalies over the Maritime Continent and the equatorial western Pacific intensify and persist (see Figures 4d–4h). These persistent convective anomalies get much weaker if a 20–100 day band-pass filter is applied (not shown), suggesting that the intraseasonal timescale variability before vortex-displacement SSWs is

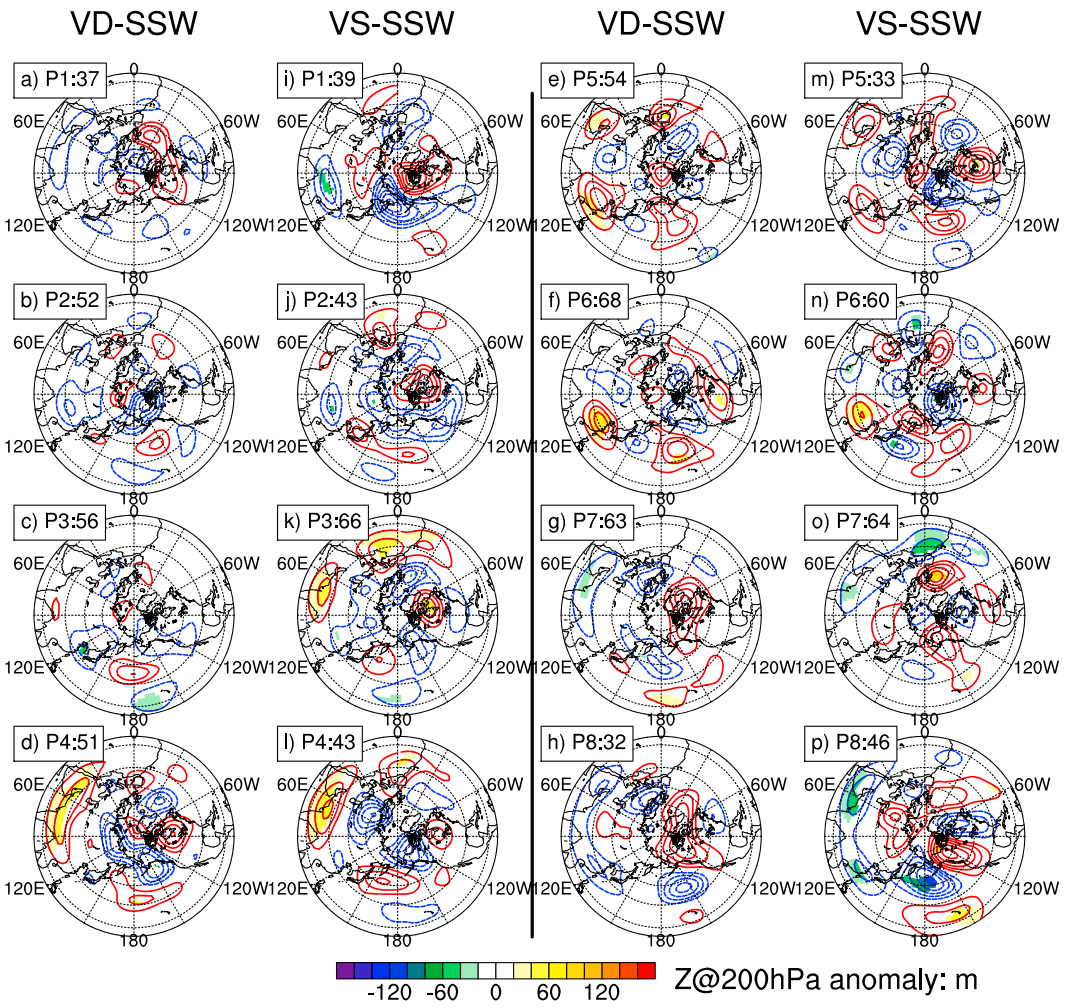

Figure 5. Same as Figure 3, but for 200 hPa geopotential height anomalies (unit: m) related to each MJO phase: (a–h) vortex-displacement SSWs; (i–p) vortex-split SSWs. Positive and negative anomalies are indicated by red solid and blue dashed contours. The contour interval is 20 m. The shaded areas are statistically significant at the 90% confidence level based on a two-tailed Student's *t* test with reduced degrees-of-freedom (see text).

less important than the variability on shorter timescales (e.g., synoptic). Therefore, the intraseasonal timescale variability may account for a larger portion of forcing of planetary waves related to vortex-split SSWs than that related to vortex-displacement SSWs. For vortex-displacement SSWs, the more active synoptic timescale variability is expected to account for the remaining portion of forcing of planetary waves.

The distinct SSW-MJO relationships shown in Figures 1 and 2 can thus be largely attributed to the different MJO features as shown in Figures 3 and 4, that is, weak convective anomalies and incoherent eastward propagation with irregular periods before vortex-displacement SSWs, but strong convective anomalies and coherent eastward propagation with regular periods before vortex-split SSWs.

3.3. Mechanism for MJO Contributions to Vortex-Displacement and Vortex-Split SSWs

G12 showed that the MJO teleconnection pattern preferentially leads to negative geopotential height anomalies over the North Pacific, which are collocated with a trough in the climatological planetary wavefield and are therefore strongly associated with upward tropospheric planetary wave driving. Therefore, they asserted that the MJO helps to enhance upward propagating planetary waves in the extratropics, which sometimes leads to SSW events in the polar stratosphere. To explore the mechanisms for the influence of MJO on different types of SSWs, we first examine MJO-related geopotential height anomalies at 200 hPa before both types of SSWs (Figure 5).

As the features of MJO are different (Figure 3), the MJO-related geopotential height anomalies are quite different during different types of SSWs (Figure 5). However, the MJO-related anomalies over the North Pacific are similar between vortex-displacement and vortex-split SSWs during most of the MJO phases. For example, there are positive anomalies over the North Pacific during MJO phases 2–6, but negative anomalies during MJO phases 7–8 and 1. Therefore, before both vortex-displacement and vortex-split SSWs, the MJO reduces the geopotential height over the North Pacific during the MJO phases 7–8 (compare Figures 5g–5h to 5o–5p). It is also noted that the geopotential height anomalies during most of the MJO phases are not statistically significant, probably because of the small sampling size in this study. According to G12, the MJOs should thus contribute to the planetary wave driving for both types of SSWs. However, the mechanism proposed by G12 was unable to explain the fundamental difference between vortex-displacement and vortex-split SSWs.

In fact, the MJO-related anomalies over the North Pacific are only the regional signatures of the MJO-related teleconnection patterns, which extend from lower latitudes toward the Arctic region. As shown in Figure 5, the MJO-related geopotential height anomalies are quite different for different types of SSWs. First, the MJO-related anomalies before vortex-split SSWs are stronger than those before vortex-displacement SSWs for most MJO phases (e.g., phases 1–3 and 5–6 and 8). This is mainly because the MJOs before vortex-split SSWs are stronger. Second, the geopotential height anomalies related to the MJO phases 7–8 show a wave number-1 pattern (i.e., one positive anomaly center over Canadian Arctic) in the Arctic during vortex-displacement SSWs (e.g., Figures 5h). In contrast, the MJO-related geopotential height anomalies show a wave number-2 pattern (i.e., one positive anomaly center over western part of North America, and the other over North Atlantic/Europe) during vortex-split SSWs (Figure 5p).

To explore the possible connection between the different features (i.e., intensity and propagation) of the MJO shown in Figure 3 and the different teleconnections associated with certain MJO phases (e.g., phase 8) shown in Figure 5, the circulation patterns related to phase 8 of different types of MJOs (i.e., weak versus strong, incoherent versus coherent) are compared. Figure 6 (top panels) compares the geopotential height anomalies related to weak and strong MJOs. The 200 hPa geopotential height anomalies are relatively weak with a wave number-1 pattern in the Arctic for weak MJOs (Figure 6a), but slightly stronger with a wave number-2 pattern in the Arctic for strong MJOs (Figure 6b). Figure 6 (central panels) compares the geopotential height anomalies related to phase 8 of incoherent and coherent eastward propagating MJOs. The MJO-related anomalies show a wave number-1 pattern in the Arctic for incoherent MJOs (Figure 6c), but a wave number-2 pattern in the Arctic for coherent MJOs (Figure 6d). Figure 6 (bottom panels) is the same as Figures 5h and 5p, comparing the MJO-related geopotential height anomalies before different types of SSWs. A quantitative analysis has been performed (but not shown) to compare the ratio between the wave number-1 and wave number-2 amplitudes for each panel in Figure 6. The results have suggested that there are stronger wave number-2 (wave number-1) anomalies for strong and coherent (weak and incoherent) MJOs and before vortex-split (vortex-displacement) SSWs. The consistency between the anomalies related to strong and coherent (weak and incoherent) MJOs and those related to MJOs before vortex-split (-displacement) SSWs suggests that differences in the intensity and propagation features of MJO may give rise to the different patterns of geopotential height anomalies associated with vortex-displacement and vortex-split SSWs. Additionally, the difference in the intensity of MJOs also contributes to the different amplitudes of the MJO-relate anomalies before vortex-displacement and vortex-split SSWs. As discussed in section 3.2, the stronger MJOs before VS SSWs are also associated with prominent negative OLR anomalies over the equatorial Atlantic Ocean in MJO phases 7–8 (see Figures 3o–3p). As a result, the strong and coherent MJOs may also contribute to the wave number-2 pattern of 200 hPa circulation anomalies over high latitudes for vortex-split SSWs by enhancing the convective anomalies in the Western Hemisphere. The patterns seen in Figures 5 and 6 show in more detail how the different characteristics of MJOs before vortex-displacement and vortex-split SSWs apparent in Figure 3 can contribute to the different behavior of the polar vortex during the two types of SSWs.

4. QBO Modulation of the MJO Teleconnection Pattern and SSW Type

Given the importance of the QBO to the upward propagation of planetary waves from the troposphere into and through the stratosphere, in this section we examine further whether QBO variability can modulate the type of SSWs by regulating MJO-related anomalies.

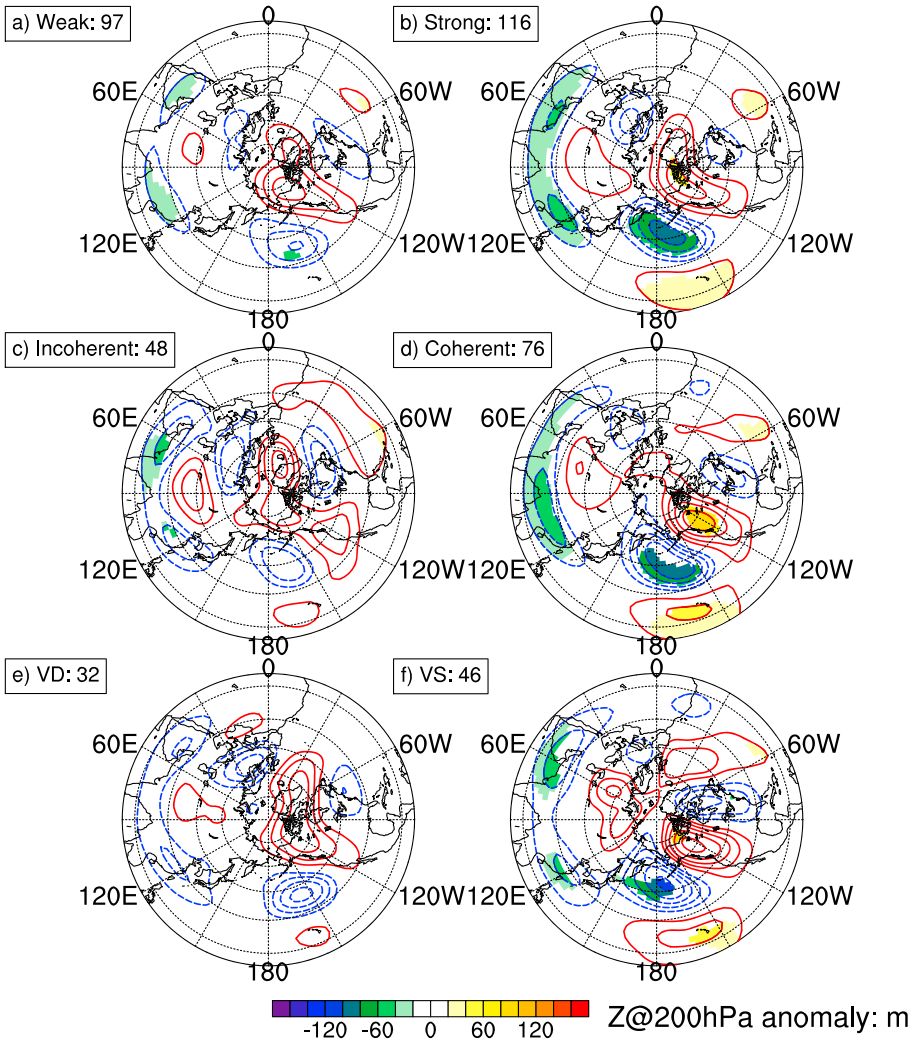

Figure 6. Same as Figure 5, but for geopotential height anomalies (unit: m) associated with the MJO phase 8: (a–b) composites for weak and strong MJOs; (c–d) composites for MJOs with incoherent and coherent propagation; (e–f) composites for MJOs before vortex-displacement and vortex-split SSWs. The definitions of weak and strong MJOs are based on the magnitude of the RMM index (i.e., smaller or larger than 1.0). The definition of incoherent and coherent MJOs is based on the propagation feature of MJO (see text).

Tables 1 and 2 show the 3 month (the month with SSW occurrence and those before and after) mean QBO indices for both types of SSWs. Ten out of the 12 vortex-displacement SSWs occur during easterly QBO phase, while six out of the eight vortex-split SSWs occur during westerly QBO phase at 50 hPa. These tables demonstrate a strong dependence of the SSW type on the QBO phase. Figure 7 (top panels) shows composites of zonal-mean zonal wind anomalies for the period 50–10 days prior to different types of SSWs. Figure 7 (lower panels) presents composites of zonal-mean zonal wind anomalies for months with easterly and westerly QBO phases. Comparison between the top and bottom panels in Figure 7 shows that the composites of zonal-mean zonal wind anomalies in the tropics before vortex-displacement

Table 2. Same as Table 1, but for the Vortex-Split SSW Events

SSW Central Dates	50 hPa
02 Jan 1985	−1.14
08 Dec 1987	0.50
14 Mar 1988	0.44
22 Feb 1989	0.32
26 Feb 1999	−0.42
18 Jan 2003	0.71
24 Jan 2009	1.09
09 Feb 2010	0.04

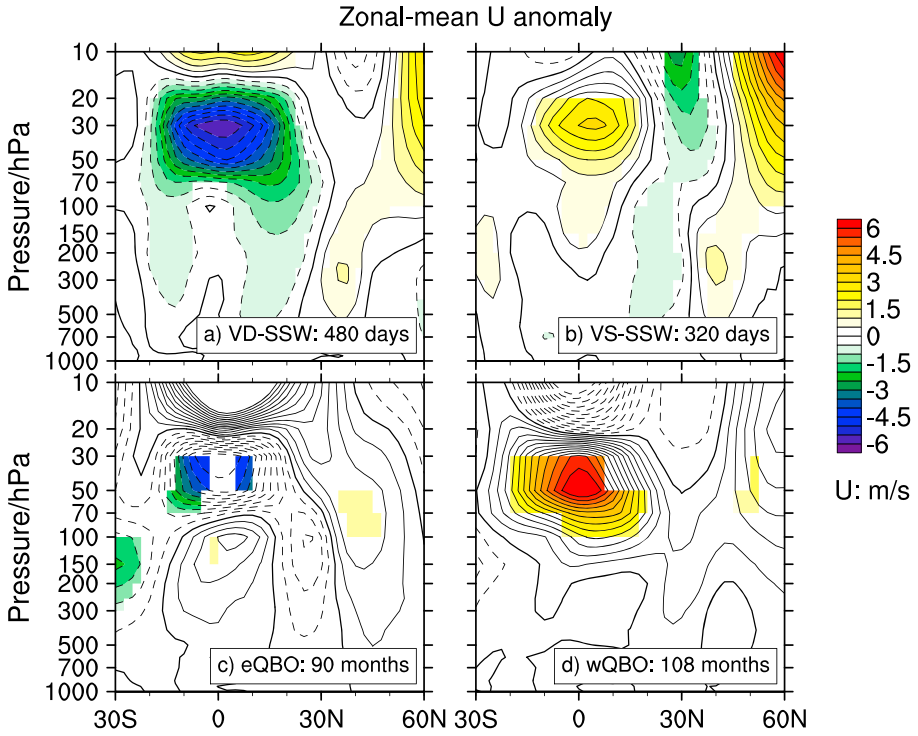

Figure 7. Composite of zonal-mean zonal wind anomalies for the period 50–10 days prior to (a) vortex-displacement and (b) vortex-split SSWs, and for months with (c) easterly and (d) westerly Quasi-Biennial Oscillation (QBO) phases during the extended winters (November–April) of 1980–2010. Positive and negative values are indicated by solid and dashed contours, respectively, with an interval of 0.5 m/s. The color-shaded (blue/green for negative, orange/yellow for positive) anomalies are statistically significant at the 95% confidence level based on a two-tailed Student's *t* test with reduced degrees-of-freedom based on the autocorrelation of the QBO index (see text). The numbers shown in the top (bottom) panels represent the number of days (months) used to construct each composite. The sampling size of each QBO phase (i.e., QBO index greater or less than 0) in lower panels is much larger than that of either vortex-displacement or vortex-split SSWs in upper panels.

and vortex-split SSWs are similar to those for easterly and westerly QBO phases, respectively. For example, before vortex-displacement SSWs, there are pronounced negative zonal-mean zonal wind anomalies in tropical stratosphere (20°S–20°N, 10–70 hPa) arching down deep into the subtropical troposphere (as low as 300–500 hPa pressure surface) in both hemispheres (Figure 7a). This resembles the case during easterly QBO phases (Figure 7c). In contrast, before vortex-split SSWs, there are relatively weak positive zonal-mean zonal wind anomalies in tropical stratosphere (20°S–20°N, 10–70 hPa) that extend down only into the altitude region between 70 and 200 hPa and even that far down only in the deep tropics (10°S–10°N) (Figure 7b). This resembles the case during westerly QBO phases (Figure 7d). These results indicate that the QBO phase may play an important role in defining the types of SSWs.

Figure 8 compares composites of MJO-related OLR anomalies during easterly and westerly QBO phases. After a two-tailed Student's *t* test with reduced degrees-of-freedom is applied, the results indicate that the MJO-related anomalies, from the equatorial Indian Ocean toward the western Pacific, during easterly QBO phases are much stronger than those during westerly QBO phases (compare left to right panels).

In the following discussion, we examine the role that the influence of QBO on 100 hPa geopotential height and wave-activity anomalies plays in the impact of MJO on both types of SSWs. Since SSWs occur following certain late MJO phases (phases 7–8), the composites of anomalies associated with MJO phases 7–8 are first compared between the two QBO phases.

Figure 9 (top panels) shows composites of 100 hPa geopotential height anomalies 1–10 days before the central dates of both types of SSWs. For vortex-split SSWs, the wave number-2 pattern of geopotential height anomalies becomes clearer, if the zonal average is removed. Therefore, to better demonstrate the fundamental difference (i.e., wave number-1 or -2 patterns of planetary disturbances) between vortex-displacement and

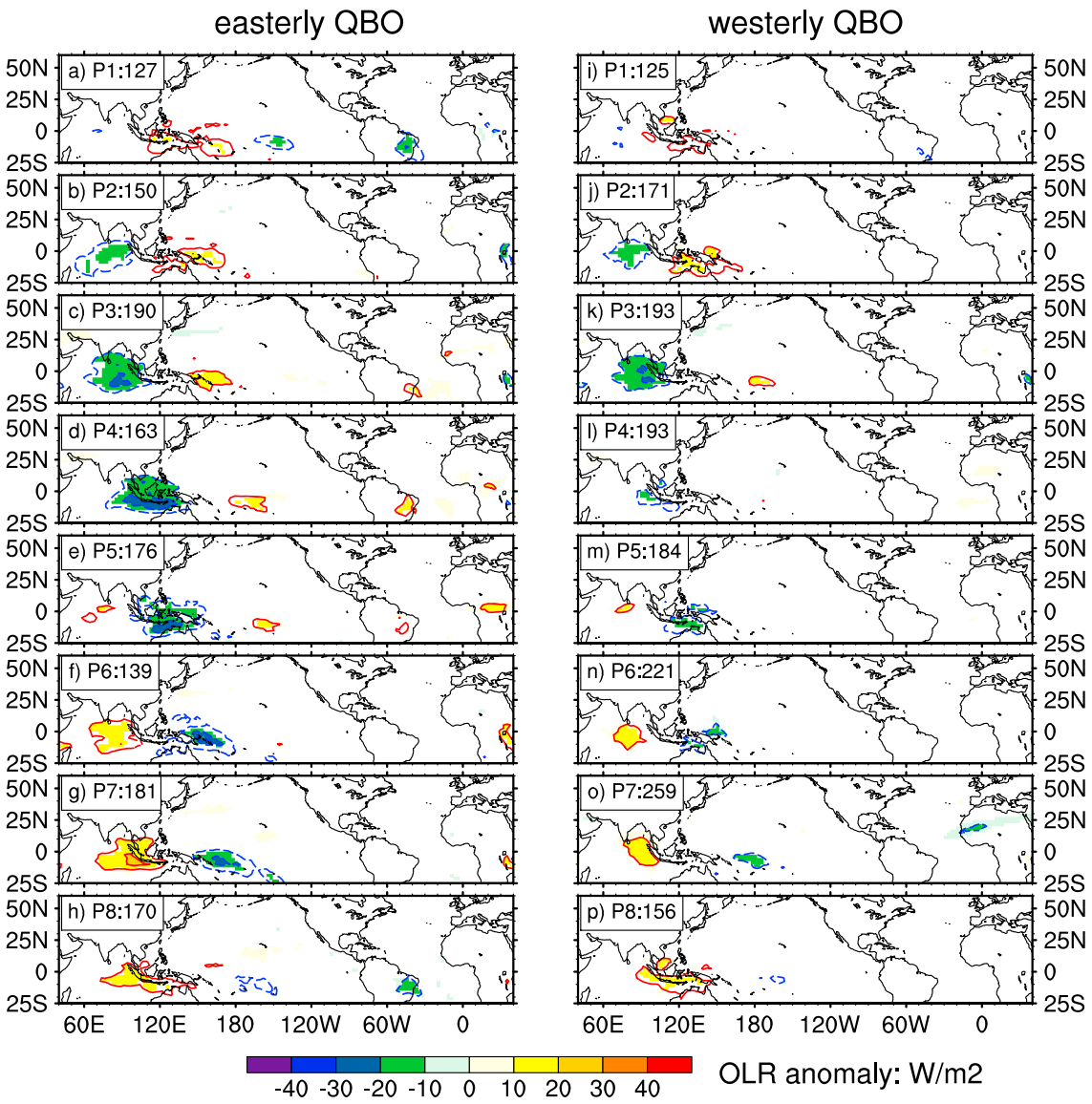

Figure 8. Same as Figure 3, but for MJO-related OLR anomalies during the easterly (left) and westerly (right) QBO phases. Sampling of easterly and westerly QBO phases is consistent with that used in Figures 7c and 7d, respectively.

vortex-split SSWs as documented in previous studies [e.g., CP07], the geopotential height anomalies with the zonal mean removed are shown in Figures 9a and 9b. Figure 9 (bottom panels) presents composites of the band-pass-filtered (20–100 days) geopotential height anomalies associated with MJO phases 7–8 during different QBO phases. Comparison of Figures 9a and 9c indicates a similar wave number-1 pattern of geopotential height anomalies in the Arctic before vortex-displacement SSWs and at MJO phases 7–8 during easterly QBO winters. Comparison of Figures 9b and 9d indicates a similar wave number-2 pattern of geopotential height anomalies in the Arctic before vortex-split SSWs and at MJO phases 7–8 during westerly QBO winters. It is noted that the amplitude of positive geopotential height anomalies over the Canadian Arctic during easterly QBO phases is greater than that during westerly QBO phases shown in Figure 9d. This difference can be attributed to differences in the intensity of the MJOs shown in Figure 8. However, the positive anomaly center over Northern Europe and Central Asia during westerly QBO phases (Figure 9d) is much stronger than that during easterly QBO (Figure 9c). Similar patterns of geopotential height anomalies are found throughout 500–50 hPa (not shown). Therefore, the QBO may play an important role in modulating the MJO-related extratropical circulation anomalies in the middle and upper troposphere and the lower stratosphere that can be important to the development of vortex-displacement versus vortex-split SSWs.

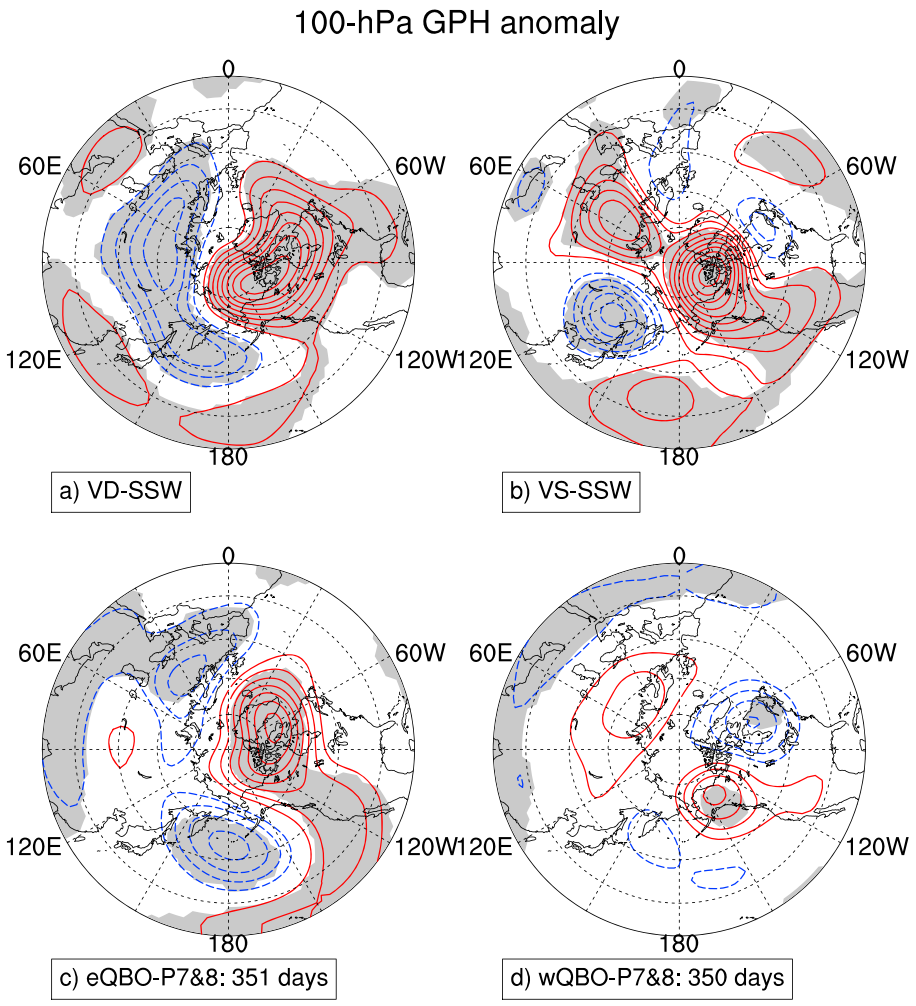

Figure 9. (a–b) Composite of 100 hPa geopotential height anomalies (zonal average removed) 1–10 days before the central dates of vortex-displacement (left) and vortex-split (right) SSWs; (c–d) band-pass-filtered (20–100 days) December–January–February geopotential height anomalies associated with the MJO phases 7–8 in the easterly (left) and westerly (right) QBO phases. The number shown in Figures 9c–9d represents the number of days used for each composite. Positive and negative anomalies are indicated by red solid and blue dashed contours. The contour interval is 20 m in top panels and 10 m in bottom panels. The shaded areas in the upper panels are statistically significant at the 90% confidence level based on a regular two-tailed Student's *t* test. The shaded areas in the lower panels are statistically significant at the 90% confidence level based on a two-tailed Student's *t* test with reduced degrees-of-freedom (see text).

The geopotential height anomalies during other MJO phases (i.e., MJO phases 1–6) have also been examined for easterly and westerly QBO phases (not shown). The results suggest that the differences in geopotential height anomalies between easterly and westerly QBO phases are fairly small during MJO phases 1–4, when the negative OLR anomalies are over the Indian Ocean. The differences become larger when the negative OLR anomalies travel across the Maritime Continent and western Pacific, during MJO phases 5–8. Therefore, it seems that the MJO can initiate planetary waves that later propagate poleward and upward into the polar stratosphere. However, this result seems inconsistent with the fact that the MJO usually becomes much weaker in its late phases (e.g., phases 7–8), when the MJO-related anomalies approach the western and central Pacific.

Given that the MJO-related anomalies are usually most active over the warm equatorial Indian Ocean (i.e., around the MJO phase 3), lagged composites of MJO-related geopotential height anomalies after MJO phase 3 are used to test whether the QBO can influence the MJO-related anomalies, which undergo further poleward and/or eastward propagation after being initiated, in the upper troposphere and lower stratosphere regions.

Figure 10 shows the lagged composites of 100 hPa geopotential height anomalies with respect to MJO phase 3 for lags of 5, 10, 15, 20, 25, and 30 days during easterly and westerly QBO phases. The patterns of MJO-related

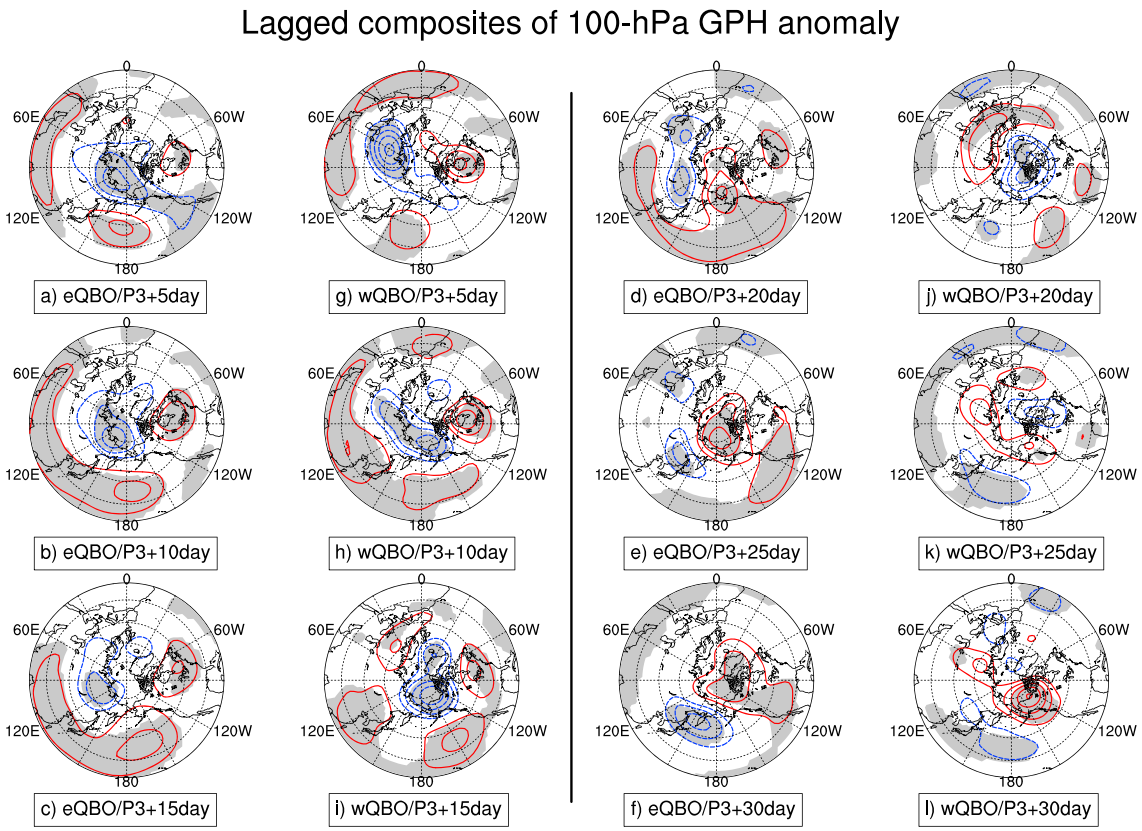

Figure 10. Lagged (+5, +10, +15, +20, +25, and +30 days) composites of 100 hPa geopotential height anomalies with respect to MJO phase 3 during the (a–f) easterly and (g–l) westerly QBO phases. The number shown below each panel represents the number of days after the MJO phase 3. Positive and negative anomalies are indicated by red solid and blue dashed contours. The contour interval is 20 m. The shaded areas are statistically significant at the 90% confidence level based on a two-tailed Student's *t* test with reduced degrees-of-freedom (see text).

anomalies between the two QBO phases are very similar at +5 and +10 days (Figures 10a–10b and 10g–10h). The main difference is that the positive anomalies over North America are stronger during westerly QBO phases than during easterly QBO phases. By +15 days, the geopotential height anomalies during the two QBO phases become different (Figures 10c and 10i). During the easterly QBO phases, the pattern at +15 days remains similar to that at +10 days (compare Figures 10c to 10b). In contrast, during the westerly QBO phases, the positive anomalies over North America have propagated along latitude circles, leading to an additional positive anomaly center over the Northern Europe (compare Figures 10i to 10h). In the following 15 days (from +15 to +30 days), the differences between the MJO-related anomalies during the two QBO phases become even more significant. For example, during easterly QBO phases, the positive anomaly center within the Arctic circle keeps developing between +20 and +30 days, producing a wave number-1 circulation pattern in the Arctic (Figures 10d–10f). The resulting wave number-1 pattern is similar to those before vortex-displacement SSWs and in MJO phases 7–8 (compare Figures 10d–10f to Figures 9a and 9c). In contrast, during westerly QBO phases, the two positive anomaly centers developed over the North Europe and Northeast Pacific from +15 to +20 days (Figure 10j), and then merged into each other from +25 to +30 in the Arctic region (Figures 10j–10l). The resulting pattern of positive anomalies looks similar to those before vortex-split SSWs and at MJO phases 7–8 (compare Figures 10j–l to Figures 9b and 9d). In addition, although the MJOs during easterly QBO phases are generally stronger than during westerly QBO phases (Figure 8), the amplitude of the MJO-related anomalies during westerly QBO phases (Figure 10l) is stronger than that during easterly QBO phases (Figure 10f). Therefore, QBO may play an important role in modulating the MJO-related circulation pattern in the Arctic.

To explore the mechanism by which the QBO can influence the MJO-related circulation patterns in the extratropics, we compare 100 hPa wave-activity flux anomalies associated with both types of SSWs, anomalies associated with MJO phases 7–8, and MJO-related anomalies 25 days after MJO phase 3 during easterly and westerly QBO phases. Figure 11 (top panels) shows composites of 100 hPa wave-activity flux

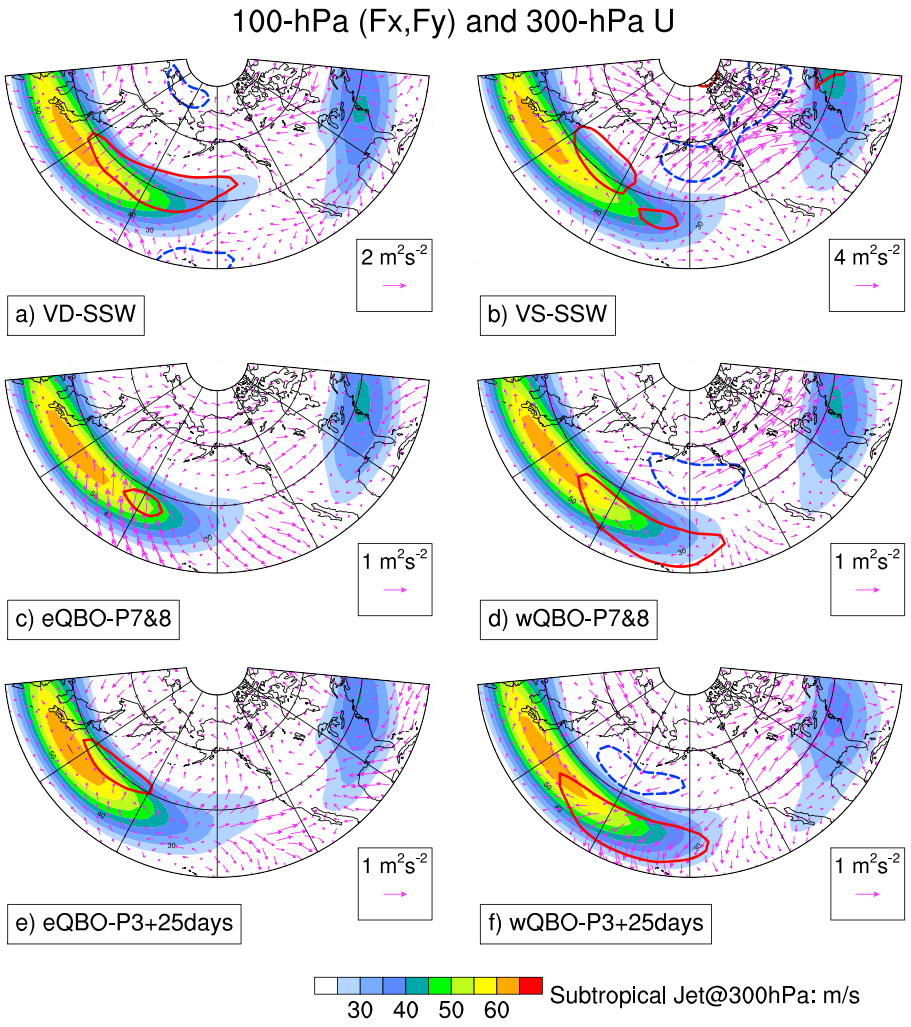

Figure 11. Horizontal wave-activity flux anomalies (100 hPa) (vectors, unit: m^2/s^{-2}) and 300 hPa zonal wind (color-shaded contours, unit: m/s): (a–b) 1–10 days before the central dates of vortex-displacement (left) and vortex-split (right) SSWs; (c–d) band-pass-filtered (20–100 days) December–January–February values associated with the MJO phases 7–8 during the easterly (left) and westerly (right) QBO phases; (e–f) band-pass-filtered (20–100 days) December–January–February values 25 days after the MJO phases 3 in the easterly (left) and westerly (right) QBO phases. Only winds greater than 25 m/s are included, with an interval of 5 m/s. Positive and negative anomalies of the 300 hPa zonal wind are indicated by red solid (+5 m/s) and blue dashed (−5 m/s) contours.

anomalies 1–10 days before the two types of SSWs. Northward wave-activity flux anomalies propagate from the tropics to the midlatitudes over the western Pacific and central Pacific Ocean before vortex-displacement and vortex-split SSWs, respectively (Figures 11a and 11b), suggesting the importance of wave disturbance sources from lower latitudes. Compared to the weak northward propagation of wave-activity fluxes over the Northwest Pacific before vortex-displacement SSWs, there is stronger northward as well as eastward propagations of wave-activity fluxes from the exit region of the subtropical jet over the Northeast Pacific toward North America before vortex-split SSWs, reminiscent of the Pacific-North-American pattern (compare Figures 11b to 11a). Figure 11 (center panels) presents the anomalous wave-activity flux vectors associated with MJO phases 7–8 during different QBO phases. There are northward wave-activity fluxes over the North and Northwest Pacific during easterly QBO phases (Figure 11c). During westerly QBO phases, the northward fluxes over the subtropical central Pacific Ocean turn eastward over the Northeast Pacific and North America. It is noted that, although the MJOs during easterly QBO phases are stronger than those during westerly QBO phases (Figure 8), there are much stronger MJO-related eastward wave-activity fluxes over the Northeast Pacific and North America during westerly QBO phases than during easterly QBO phases (compare Figures 11d to 11c). The difference in the propagation of the wave-activity fluxes is pronounced between

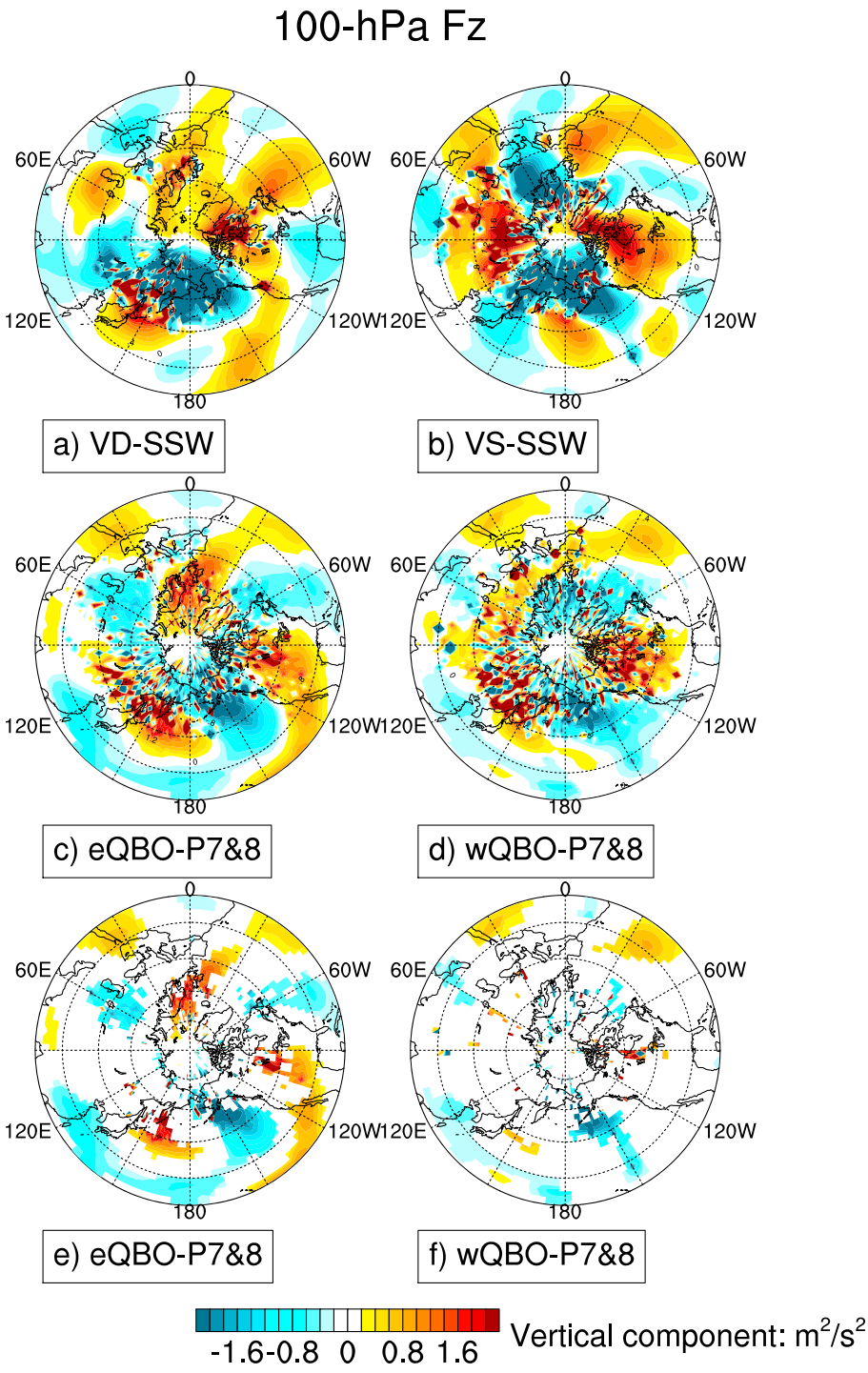

Figure 12. Vertical wave-activity flux anomalies (unit: m^2/s^{-2}) at the 100 hPa pressure surface: (a–b) 1–10 days before the central dates of vortex-displacement (left) and vortex-split (right) SSWs; (c–d) band-pass-filtered (20–100 days) December–January–February values associated with the MJO phases 7–8 in the easterly (left) and westerly (right) QBO phases; (e–f) same as Figures 12c–12d, but cases that are statistically significant at the 90% confidence level based on a two-tailed Student's *t* test with reduced degrees-of-freedom (see text).

different QBO phases, in a pattern that echoes the difference between propagation prior to different types of SSWs (compare central to top panels). Similar patterns of differences in wave-activity flux anomalies occur up to 50 hPa (not shown). Figure 11 (bottom panels) shows the MJO-related wave-activity flux vectors 25 days after MJO phase 3 during different QBO phases. During easterly QBO phases, the MJO-related wave-activity

fluxes propagate northward from the tropics toward the North Pacific and the Bering Sea, and are consistent with those before vortex-displacement SSWs and those associated with MJO phases 7–8 during easterly QBO phases (compare Figure 11e to Figures 11a and 11c). During westerly QBO phases, there are eastward fluxes over North America toward North Atlantic (Figure 11f). Although the pattern shown in Figure 11f is slightly different from those shown in Figures 11b and 11d, it highlights the eastward/downstream propagating anomalous wave-activity fluxes over the North America shown in Figures 11b and 11d.

Figure 12 shows the vertical component of the wave-activity flux anomalies. Generally, there are wave number-1 patterns of the vertical component of wave-activity flux before vortex-displacement SSWs (Figure 12a) and during easterly QBO phases (Figure 12c). For example, there are upward anomalous fluxes over the Canadian Arctic, the North Atlantic, Northern Europe, and the Northwest Pacific, but downward anomalous fluxes over the Russian Far East, the Bering Sea, and Alaska. In contrast, there are wave number-2 patterns of the vertical component of wave-activity flux before vortex-split SSWs (Figure 12b) and during westerly QBO phases (Figure 12d). For example, there are upward anomalous fluxes over North America and the Eurasian Arctic, but downward anomalous fluxes over the Bering Sea/Alaska and Northern Europe. As a result of the climatological mean has been removed, the daily anomalous fluxes appear spotty (top panels). After the band-pass filtering applied, the MJO-related anomalies become even more spotty (center panels). The bottom panels suggest that very few MJO-related anomalies shown in the center panels are statistically significant at the 90% confidence level, based on a two-tailed Student's *t* test with reduced degrees-of-freedom applied. This can be probably attributed to the fact that the upward propagation of planetary waves is also modulated by factors other than QBO phases.

Previous studies have shown that the extratropical propagation of Rossby waves follows a great circle track [e.g., *Hoskins and Karoly*, 1981] that is modulated by the subtropical jet streams [e.g., *Hoskins and Ambrizzi*, 1993]. The upper tropospheric subtropical jet streams are compared between different types of SSWs and between different QBO phases. Some apparent differences are found at the exit region of the jets, especially over the Pacific Ocean. These anomalies at the jet exit regions are highlighted by red solid and blue dashed contours in Figure 11. Compared to that prior to vortex-displacement SSW, the subtropical jet shows a more equatorward shift at the Pacific exit region (compare Figures 11a to 11b). There are also apparent differences in the upper tropospheric subtropical jet between the two QBO phases that are very similar to those between vortex-displacement and vortex-split SSWs (compare center/bottom panels to top panels). Compared to easterly QBO phases, the subtropical jet shows a more equatorward shift at its Pacific exit region during westerly QBO phases (compare Figures 11c and 11e to 11d and 11f). These differences in the subtropical jet between different QBO phases are consistent with those reported by *Garfinkel and Hartmann* [2011a, 2011b]. Given that the horizontal and vertical components of the wave-activity fluxes should be dynamically coupled with each other, the QBO may modulate the poleward and upward propagation of enhanced planetary waves initiated by the MJO convective anomalies via its influence on the subtropical westerly jet in the upper troposphere. As shown in the present study, during easterly QBO phases, the subtropical jet directs the MJO-related wave-activity fluxes northward (Figures 11c and 11e) and leads to wave number-1 pattern of vertical component of wave-activity fluxes at high latitudes (Figure 12c). In contrast, during westerly QBO phases, the subtropical jet directs the MJO-related wave-activity fluxes eastward (Figures 11d and 11f) and leads to wave number-2 pattern of vertical component of wave-activity fluxes at high latitudes (Figure 12d). As a result, there are more vortex-displacement (-split) SSWs during easterly (westerly) QBO phases (Table 1).

5. Summary and Discussion

We have examined the connection between the equatorial MJO and different types (i.e., vortex-displacement and vortex-split) of NH mid-winter major SSWs during 1980–2010. The results indicate that the MJO-SSW relationships are quite different for different types of SSWs. A well-defined in-phase relationship between the eastward propagation of the MJO at different lead times before the central dates of SSWs is found for vortex-split SSWs but not for vortex-displacement SSWs. The MJO is more strongly linked to vortex-split SSWs than to vortex-displacement SSWs, with a connection seen up to 48 days prior to the central dates of vortex-split SSWs. The different MJO-SSW relationships can largely be attributed to the different features of MJO before different types of SSWs. Composite analysis indicates that, the MJOs before vortex-split SSWs are stronger and show more coherent eastward propagation with regular periods than those before vortex-displacement

SSWs. As a result, the intraseasonal timescale variability accounts for a larger portion of the planetary wave forcing related to vortex-split SSWs than it does to that related to vortex-displacement SSWs.

MJOs before vortex-displacement and vortex-split SSWs can both reduce the geopotential height over the North Pacific in late phases (e.g., phases 7–8). Therefore, the mechanism proposed by G12 involving such reduced geopotential heights does not explain the different MJO-SSW relationships for different types of SSWs. Composite analysis indicates that weaker and incoherent MJOs lead to a more poleward wave-train pattern over the North Pacific and North American sector, which is more commonly associated with a wave number-1 pattern of circulation anomalies in the Arctic. In contrast, stronger and coherent MJOs lead to a more eastward wave-train pattern and are associated with a wave number-2 pattern of anomalies in the Arctic. The intensity and propagation features of MJO may thus play a role in shaping the MJO-related circulation patterns in the Arctic.

A strong dependence of SSW category on QBO phase has been revealed. Vortex-displacement (-split) SSWs preferentially occur during easterly (westerly) QBO phases. Composites show that there are wave number-1 (-2) patterns of geopotential height anomalies associated with MJO phases 7–8 in the Arctic during easterly (westerly) QBO phases, which resemble those associated with vortex-displacement (-split) SSWs. Different patterns of wave-activity flux anomalies may play important roles in modulating the different patterns of geopotential height anomalies related to different types of SSWs and those related to MJO during different QBO phases. Northward anomalous wave-activity fluxes are found over the Northwest Pacific before vortex-displacement SSWs, and during easterly QBO phases (related to MJO phases 7–8, or ~25–30 days after phase 3). In contrast, more eastward anomalous wave-activity fluxes are found over the Northeast Pacific and North American sectors before vortex-split SSWs, and during westerly QBO phases (related to MJO phases 7–8, or ~25–30 days after phase 3). Composite analysis suggests that the amplitude of MJOs during easterly QBO phases is much stronger than that during westerly QBO phases. However, it does not explain the fact that some of the MJO-related anomalies (e.g., geopotential height anomalies in the Arctic, eastward wave-activity fluxes over North America) during westerly QBO phases are stronger than those during easterly QBO phases. Therefore, the QBO could play an important role in modulating MJO-related anomalies (e.g., geopotential height and wave-activity flux) in the Arctic. Further analysis suggests that the MJO-related anomalies in the Arctic are very likely initiated when the MJO-related convective anomalies are active over the equatorial Indian Ocean (around MJO phase 3).

It is also found that the upper tropospheric subtropical jet streams, which modulate the propagation of Rossby waves, are quite different, especially at their Pacific exit region, during easterly and westerly QBO phases. Therefore, it is proposed that the QBO may modulate the poleward and upward propagation of MJO-related wave disturbances via its influence on the upper tropospheric subtropical jet over the central and eastern Pacific Ocean. However, further studies using both observations and models are needed to verify this proposed mechanism. It will also be interesting to investigate how the solar cycle can influence the QBO modulation of the MJO-related anomalies in the extratropics, and thus in turn influence the type of SSWs.

Although well-defined MJO-SSW relationships have been presented here, the number of major SSWs (of either vortex-displacement or vortex-split type) is much smaller than the number of wintertime periods with strong MJOs. Since only major mid-winter SSWs have been considered in the present study, it is possible that MJO-related anomalies alone frequently do not reach sufficiently large amplitudes to induce major SSWs. For example, in this study, we have found that the convective anomalies associated with synoptic timescale variability may also be important for vortex-displacement SSWs. We have examined additional vortex-displacement and vortex-split events, which do not necessarily lead to major SSWs [e.g., *Mitchell et al.,* 2013; *Seviour et al.,* 2013]. The results have indicated that the MJO-SSW relationship obtained in this study does not apply to all polar vortex disturbance events (not shown). This indicates that, in addition to the influences of QBO and MJO, the occurrence and characteristics of SSWs are affected by other forcings (such as the synoptic scale disturbances, atmospheric instabilities, solar cycle, SST, and snow cover), and by preconditioning of the polar vortex that may depend on multiple forcings well in advance of the SSW. Furthermore, poleward and upward propagation of the planetary waves is also modulated by other underlying conditions, such as variations of the subtropical upper tropospheric jet and polar night jet that affect the refractive index. Further studies are needed to explore these possibilities.

Stratospheric anomalies related to SSWs have long been believed to play a crucial role in improving extended-range weather forecasts [e.g., *Baldwin and Dunkerton,* 2001; *Sigmond et al.,* 2013]. In this study, we

have demonstrated a QBO-sensitive linkage between NH mid-winter major SSWs and the tropical MJO, which is also a major factor influencing seasonal predictability. It will be interesting and important to test how well the relationship between the MJO, QBO, and SSWs is represented in stratosphere-resolving atmospheric models. Improvement of SSW prediction based on the MJO-SSW relationship and the predictability of the MJO could extend seasonal weather predictability in future state-of-the-art weather forecast models. Because of the high sensitivity of the MJO-related circulation pattern to the phase of the QBO, accurate representation of QBO in forecast models will be a prerequisite for simulating and predicting the global influences of MJO.

Acknowledgments

This research was supported by the National Science Foundation award ATM-0840755 to University of California, Los Angeles. Part of this research was carried out at the Jet Propulsion Laboratory, California Institute of Technology, under a contract with the National Aeronautics and Space Administration. KFL was supported by the Jack Eddy Fellowship, managed by the University Corporation for Atmospheric research. We thank George Kiladis and two anonymous reviewers for their helpful comments. We thank Guang J. Zhang for helpful discussions. The NCEP-NCAR reanalysis data were kindly provided by the NOAA/OAR/ESRL-PSD, Boulder, Colorado, from their website (http://www.esrl.noaa.gov/psd/).

References

Andrews, D. G., J. R. Holton, and C. B. Leovy (1987), *Middle Atmosphere Dynamics*, 489 pp., Academic Press, San Diego, Calif.

Baldwin, M. P., and T. J. Dunkerton (2001), Stratospheric harbingers of anomalous weather regimes, *Science*, *294*, 581–584.

Baldwin, M. P., et al. (2001), The quasi-biennial oscillation, *Rev. Geophys.*, *39*, 179–229, doi:10.1029/1999RG000073.

Bell, C. J., L. J. Gray, A. J. Charlton-Perez, M. M. Joshi, and A. A. Scaife (2009), Stratospheric communication of El Niño teleconnections to European winter, *J. Clim.*, *22*, 4083–4096.

Butler, A. H., and L. M. Polvani (2011), El Niño, La Niña, and stratospheric sudden warmings: A reevaluation in light of the observational record, *Geophys. Res. Lett.*, *38*, L13807, doi:10.1029/2011GL048084.

Camp, C. D., and K. K. Tung (2007), The influence of the solar cycle and QBO on the late-winter stratospheric polar vortex, *J. Atmos. Sci.*, *4*, 1267–1283.

Cassou, C. (2008), Intraseasonal interaction between the Madden-Julian Oscillation and the North Atlantic Oscillation, *Nature*, *455*, 523–527.

Castanheira, J. M., and D. Barriopedro (2010), Dynamical connection between tropospheric blockings and stratospheric polar vortex, *Geophys. Res. Lett.*, *37*, L13809, doi:10.1029/2010GL043819.

Charlton, A. J., and L. M. Polvani (2007), A new look at stratospheric sudden warmings. Part I: Climatology and modeling benchmarks, *J. Clim.*, *20*, 449–469.

Cohen, J., and J. Jones (2011), Tropospheric precursors and stratospheric warmings, *J. Clim.*, *24*, 6562–6572.

García-Herrera, R., N. Calvo, R. R. Garcia, and M. A. Giorgetta (2006), Propagation of ENSO temperature signals into the middle atmosphere: A comparison of two general circulation models and ERA-40 reanalysis data, *J. Geophys. Res.*, *111*, D06101, doi:10.1029/2005JD006061.

Garfinkel, C. I., and D. L. Hartmann (2011a), The influence of the quasi-biennial oscillation on the troposphere in winter in a hierarchy of models. Part I: Simplified dry GCMs, *J. Atmos. Sci.*, *68*, 1273–1289.

Garfinkel, C. I., and D. L. Hartmann (2011b), The influence of the quasi-biennial oscillation on the troposphere in winter in a hierarchy of models. Part II: Perpetual winter WACCM runs, *J. Atmos. Sci.*, *68*, 2026–2041.

Garfinkel, C. I., D. L. Hartmann, and F. Sassi (2010), Tropospheric precursors of anomalous Northern Hemisphere stratospheric polar vortices, *J. Clim.*, *23*, 3282–3299.

Garfinkel, C. I., A. H. Butler, D. W. Waugh, M. M. Hurwitz, and L. M. Polvani (2012a), Why might stratospheric sudden warmings occur with similar frequency in El Niño and La Niña winters?, *J. Geophys. Res.*, *117*, D19106, doi:10.1029/2012JD017777.

Garfinkel, C. I., S. B. Feldstein, D. W. Waugh, C. Yoo, and S. Lee (2012b), Observed connection between stratospheric sudden warmings and the Madden-Julian Oscillation, *Geophys. Res. Lett.*, *39*, L18807, doi:10.1029/2012GL053144.

Garfinkel, C. I., T. A. Shaw, D. L. Hartmann, and D. W. Waugh (2012c), Does the Holton–Tan mechanism explain how the quasi-biennial oscillation modulates the arctic polar vortex?, *J. Atmos. Sci.*, *69*, 1713–1733.

Gill, A. E. (1980), Some simple solutions for heat-induced tropical circulation, *Q. J. R. Meteorol. Soc.*, *106*, 447–462.

Gruber, A., and A. F. Krueger (1984), The status of the NOAA outgoing longwave radiation data set, *Bull. Am. Meteorol. Soc.*, *65*, 958–962.

Hamilton, K. P. (1993), An examination of observed Southern Oscillation effects in the Northern Hemisphere stratosphere, *J. Atmos. Sci.*, *50*(20), 3468–3473.

Hendon, H. H., and M. L. Salby (1996), Planetary-scale circulations forced by intraseasonal variations of observed convection, *J. Atmos. Sci.*, *53*, 1751–1758.

Holton, J. R., and J. Austin (1991), The influence of the equatorial QBO on sudden stratospheric warmings, *J. Atmos. Sci.*, *48*, 607–618.

Holton, J. R., and H.-C. Tan (1980), The influence of the equatorial quasi-biennial oscillation on the global circulation at 50 mb, *J. Atmos. Sci.*, *37*, 2200–2208.

Holton, J. R., and H.-C. Tan (1982), The quasi-biennial oscillation in the Northern Hemisphere lower stratosphere, *J. Meteorol. Soc. Jpn.*, *60*, 140–148.

Hoskins, B. J., and T. Ambrizzi (1993), Rossby wave propagation on a realistic longitudinally varying flow, *J. Atmos. Sci.*, *50*, 1661–1671.

Hoskins, B. J., and D. J. Karoly (1981), The steady linear response of a spherical atmosphere to thermal and orographic forcing, *J. Atmos. Sci.*, *38*, 1179–1196.

Hsu, H. H. (1996), Global view of the intraseasonal oscillation during northern winter, *J. Clim.*, *9*, 2386–2406.

Kalnay, E., et al. (1996), The NCAR/NCEP 40-year reanalysis project, *Bull. Am. Meteorol. Soc.*, *77*, 437–471.

Kiladis, G. N., K. H. Straub, G. C. Reid, and K. S. Gage (2001), Aspects of interannual and intraseasonal variability of the tropopause and lower stratosphere, *Q. J. R. Meteorol. Soc.*, *127*, 1961–1983.

Kiladis, G. N., J. Dias, K. H. Straub, M. C. Wheeler, S. N. Tulich, K. Kikuchi, K. M. Weickmann, and M. J. Ventrice (2014), A comparison of OLR and circulation-based indices for tracking the MJO, *Mon. Weather Rev.*, *142*, 1697–1715.

Labitzke, K. (1965), On the mutual relation between stratosphere and troposphere during periods of stratospheric warmings in winter, *J. Appl. Meteorol.*, *4*, 91–99.

Labitzke, K. (1987), Sunspots, the QBO, and the stratospheric temperature in the north polar region, *Geophys. Res. Lett.*, *14*, 535–537, doi:10.1029/GL014i005p00535.

Labitzke, K., and M. Kunze (2009), On the remarkable Arctic winter in 2008/2009, *J. Geophys. Res.*, *114*, D00I02, doi:10.1029/2009JD012273.

Labitzke, K., and H. van Loon (1988), Association between the 11-year solar cycle, the QBO and the atmosphere. Part I: The troposphere and stratosphere in the Northern Hemisphere in winter, *J. Atmos. Terr. Phys.*, *50*, 197–206.

Labitzke, K., M. Kunze, and S. Brönnimann (2006), Sunspots, the QBO, and the stratosphere in the north polar region—20 years later, *Meteorol. Z.*, *15*, 355–363.

Lau, W. K. M., and D. E. Waliser (Eds.) (2012), *Intraseasonal Variability in the Atmosphere-Ocean Climate System,* 2nd ed., 581 pp., Springer, Heidelberg, Germany.
Leovy, C. B., C. Sun, M. H. Hitchman, E. E. Remsberg, J. M. Russell, L. L. Gordley, J. C. Gille, and L. V. Lyjak (1985), Transport of ozone in the Middle stratosphere: Evidence for planetary wave breaking, *J. Atmos. Sci.*, *42*, 230–244.
L'Heureux, M. L., and R. W. Higgins (2008), Boreal winter links between the Madden–Julian Oscillation and the Arctic Oscillation, *J. Clim.*, *21*, 3040–3050.
Li, K.-F., and K.-K. Tung (2014), Quasi-biennial oscillation and solar cycle influences on winter Arctic total ozone, *J. Geophys. Res. Atmos.*, *119*, 5823–5835, doi:10.1002/2013JD021065.
Liebmann, B., and C. A. Smith (1996), Description of a complete (interpolated) outgoing longwave radiation dataset, *Bull. Am. Meteorol. Soc.*, *77*, 1275–1277.
Lin, H., G. Brunet, and J. Derome (2009), An observed connection between the North Atlantic Oscillation and the Madden–Julian Oscillation, *J. Clim.*, *22*, 364–380.
Liu, Y., C. X. Liu, H. P. Wang, X. X. Tie, S. T. Gao, D. Kinnison, and G. Brasseur (2009), Atmospheric tracers during the 2003–2004 stratospheric warming event and impact of ozone intrusions in the troposphere, *Atmos. Chem. Phys.*, *9*, 2157–2170.
Madden, R. A., and P. R. Julian (1972), Description of global-scale circulation cells in tropics with a 40–50 day period, *J. Atmos. Sci.*, *29*(6), 1109–1123.
Manney, G. L., J. D. Farrara, and C. R. Mechoso (1994), Simulations of the February 1979 stratospheric sudden warming: Model comparisons and three-dimensional evolution, *Mon. Weather Rev.*, *122*, 1115–1140.
Manney, G. L., J. L. Sabutis, D. R. Allen, W. A. Lahoz, A. A. Scaife, C. E. Randall, S. Pawson, B. Naujokat, and R. Swinbank (2005), Simulations of dynamics and transport during the September 2002 Antarctic major warming, *J. Atmos. Sci.*, *62*, 690–707.
Manney, G. L., et al. (2009), Satellite observations and modeling of transport in the upper troposphere through the lower mesosphere during the 2006 major stratospheric sudden warming, *Atmos. Chem. Phys.*, *9*, 4775–4795.
Manzini, E., M. A. Giorgetta, M. Esch, L. Kornblueh, and E. Roeckner (2006), The influence of sea surface temperatures on the northern winter stratosphere: Ensemble simulations with the MAECHAM5 model, *J. Clim.*, *19*, 3863–3881.
Martius, O., L. M. Polvani, and H. C. Davies (2009), Blocking precursors to stratospheric sudden warming events, *Geophys. Res. Lett.*, *36*, L14806, doi:10.1029/2009GL038776.
Matsuno, T. (1966), Quasi-geostrophic motions in the equatorial area, *J. Meteorol. Soc. Jpn.*, *44*, 25–43.
Matthewman, N. J., J. G. Esler, A. J. Charlton-Perez, and L. M. Polvani (2009), A new look at stratospheric sudden warmings. Part III: Polar vortex evolution and vertical structure, *J. Clim.*, *22*, 1566–1585.
Matthews, A. J., B. J. Hoskins, and M. Masutani (2004), The global response to tropical heating in the Madden–Julian oscillation during the northern winter, *Q. J. R. Meteorol. Soc.*, *130*, 1991–2011.
McLandress, C., J. F. Scinocca, T. G. Shepherd, M. C. Reader, and G. L. Manney (2013), Dynamical control of the mesosphere by orographic and nonorographic gravity wave drag during the extended Northern winters of 2006 and 2009, *J. Atmos. Sci.*, *70*, 2152–2169.
Mitchell, D. M., L. J. Gray, J. Anstey, M. P. Baldwin, and A. J. Charlton (2013), The influence of stratospheric vortex displacements and splits on surface climate, *J. Clim.*, *26*, 2668–2682.
Mori, M., and M. Watanabe (2008), The growth and triggering mechanism of the PNA: A MJO–PNA coherence, *J. Meteorol. Soc. Jpn.*, *86*, 213–236.
Nishii, K., H. Nakamura, and T. Miyasaka (2009), Modulations in the planetary wave field induced by upward-propagating Rossby wave packets prior to stratospheric sudden warming events: A case study, *Q. J. R. Meteorol. Soc.*, *135*, 39–52.
O'Neill, A. (2003), Middle atmosphere: Stratospheric sudden warmings, in *Encyclopedia of Atmospheric Sciences*, edited by J. R. Holton, J. A. Pyle, and J. A. Curry, pp. 1342–1353, Academic, Amsterdam, London.
O'Neill, A., and B. F. Taylor (1979), A study of the major stratospheric warming of 1976/77, *Q. J. R. Meteorol. Soc.*, *105*, 71–92.
Quiroz, R. S. (1986), The association of stratospheric warmings with tropospheric blocking, *J. Geophys. Res.*, *91*, 5277–5285, doi:10.1029/JD091iD04p05277.
Rui, H., and B. Wang (1990), Development characteristics and dynamic structure of tropical intraseasonal convection anomalies, *J. Atmos. Sci.*, *47*(3), 357–379.
Sassi, F., D. Kinnison, B. A. Boville, R. R. Garcia, and R. Roble (2004), Effect of El Niño–Southern Oscillation on the dynamical, thermal, and chemical structure of the middle atmosphere, *J. Geophys. Res.*, *109,* D17108, doi:10.1029/2003JD004434.
Seviour, W. J. M., D. M. Mitchell, and L. J. Gray (2013), A practical method to identify displaced and split stratospheric polar vortex events, *Geophys. Res. Lett.*, *40*, 5268–5273, doi:10.1002/grl.50927.
Sigmond, M., J. F. Scinocca, V. V. Kharin, and T. G. Shepherd (2013), Enhanced seasonal forecast skill following stratospheric sudden warmings, *Nat. Geosci.*, *6*, 98–102.
Simmons, A. J., J. M. Wallace, and G. W. Branstator (1983), Barotropic wave propagation and instability, and atmospheric teleconnection patters, *J. Atmos. Sci.*, *40*, 1363–1392.
Straub, K. H. (2013), MJO initiation in the real-time multivariate MJO index, *J. Clim.*, *26*, 1130–1151.
Taguchi, M., and D. L. Hartmann (2006), Increased occurrence of stratospheric sudden warmings during El Niño as simulated by WACCM, *J. Clim.*, *19*, 324–332.
Takaya, K., and H. Nakamura (2001), A formulation of a phase-independent wave-activity flux for stationary and migratory quasigeostrophic eddies on a zonally varying basic flow, *J. Atmos. Sci.*, *58*, 608–627.
Tian, B., D. E. Waliser, R. A. Kahn, and S. Wong (2011), Modulation of Atlantic aerosols by the Madden-Julian Oscillation, *J. Geophys. Res.*, *116*, D15108, doi:10.1029/2010JD015201.
van Loon, H., and K. Labitzke (1987), The Southern Oscillation. Part V: The anomalies in the lower stratosphere of the Northern Hemisphere in winter and a comparison with the Quasi-Biennial Oscillation, *Mon. Weather Rev.*, *115*, 357–369.
van Loon, H., C. S. Zerefos, and C. C. Repapis (1982), The Southern Oscillation in the stratosphere, *Mon. Weather Rev.*, *110*, 225–229.
Waliser, D. E. (2012), Predictability and forecasting, in *Intraseasonal Variability in the Atmosphere-Ocean Climate System*, 2nd ed., edited by W. K. M. Lau and D. E. Waliser, pp. 433–476, Springer, Berlin, Heidelberg.
Weare, B. C. (2010), Extended Eliassen-Palm fluxes associated with the Madden-Julian oscillation in the stratosphere, *J. Geophys. Res.*, *115*, D24103, doi:10.1029/2010JD014390.
Wheeler, M. C., and H. H. Hendon (2004), An all-season real-time multivariate MJO index: Development of an index for monitoring and prediction, *Mon. Weather Rev.*, *132*, 1917–1932.
Zhang, C. (2005), Madden-Julian Oscillation, *Rev. Geophys.*, *43*, RG2003, doi:10.1029/2004RG000158.
Zhang, C. (2013), Madden–Julian Oscillation: Bridging weather and climate, *Bull. Am. Meteorol. Soc.*, *94*, 1849–1870.
Zhou, S., and A. J. Miller (2005), The interaction of the Madden–Julian Oscillation and the Arctic Oscillation, *J. Clim.*, *18*, 143–159.